Since January 2020 Elsevier has created a COVID-19 resource centre with free information in English and Mandarin on the novel coronavirus COVID-19. The COVID-19 resource centre is hosted on Elsevier Connect, the company's public news and information website.

Elsevier hereby grants permission to make all its COVID-19-related research that is available on the COVID-19 resource centre - including this research content - immediately available in PubMed Central and other publicly funded repositories, such as the WHO COVID database with rights for unrestricted research re-use and analyses in any form or by any means with acknowledgement of the original source. These permissions are granted for free by Elsevier for as long as the COVID-19 resource centre remains active.

Sustainable Cities and Society 75 (2021) 103263

Contents lists available at ScienceDirect

Sustainable Cities and Society

journal homepage: www.elsevier.com/locate/scs

The case of Tehran's urban heat island, Iran: Impacts of urban 'lockdown' associated with the COVID-19 pandemic

Gholamreza Roshan [a,*], Reza Sarli [a], Stefan W. Grab [b]

[a] Department of Geography, Golestan University, Shahid Beheshti, Gorgan 49138-15759, Iran
[b] School of Geography, Archaeology and Environmental Studies, University of the Witwatersrand, Private Bag 3, Wits, Johannesburg 2050, South Africa

ARTICLE INFO

Keywords:
COVID-19 pandemic
Urban heat island
Temperature departures
Tehran metropolis

ABSTRACT

The increasing expansion of urban environments with associated transformation of land-cover has led to the formation of urban heat islands (UHI) in many urbanized regions worldwide. COVID-19 related environmental impacts, through reduced urban activities, is worthy of investigation as it may demonstrate human capacity to manage UHI. We aim to establish the thermal impacts associated with COVID-19 induced urban 'lockdown' from 20 March to 20 April 2020 over Tehran. Areal changes in UHI are assessed through Classification and Regression Trees (CART), measured against background synoptic scale temperature changes over the years 1950–2020. Results indicate that monthly $T_{mean,}$ T_{max} and T_{min} values during this time were considerably lower than long-term mean values for the reference period. Although the COVID-19 initiated shutdown led to an identifiable temperature anomaly, we demonstrate that this is not a product of upper atmospheric or synoptic conditions alone. We also show that the cooling effect over Tehran was not spatially uniform, which is likely due to the complexity of land uses such as industrial as opposed to residential. Our findings provide potentially valuable insights and implications for future management of urban heat islands during extreme heat waves that pose a serious threat to human health.

1. Introduction

There has been continued and rapid global expansion of urban environments with associated human activities (e.g. vehicular /air traffic), industrial outputs and land-cover transformation into the built-environment over recent years (Senanayake, Welivitiya, & Nadeeka, 2013; Soydan, 2020, Yamamoto & Ishikawa, 2020; Ahmed, Ahmad, & Jeon, 2021). A consequence of this is greater differentiation in atmospheric energy balances between the built environment and immediate surrounding natural environment. Consequently, built-up city regions may experience mean air temperatures of up to a few degrees Celsius higher than surrounding sub-urban and naturally vegetated areas - a phenomenon commonly referred to as 'urban heat islands' (UHI) (e.g. Silva, DaSilva, & GuimarãesSantos, 2018; Yao et al., 2020; Zhou et al., 2020; Geraldi et al., 2021). UHI are affected by urban planning policies that include, amongst others, the replacement of vegetation with artificial structures. In addition to causing environmental pollution, the built environment also contributes to localized climate and ecological change (László Bart, 2010; Emadodin, Taravat, & Rajaei, 2016; Inostroza and PeileiFan, 2019; Ankur and Shweta Bhati, 2020). The relatively dark surfaces of buildings, streets and other paved areas typically have lower reflectance (albedo) than natural vegetated surfaces (Jiang et al., 2020). Built surfaces absorb greater amounts of incoming solar radiation, which is then converted into thermal energy, thus increasing perceptible heat in the surrounding environment (i.e. 'heat islands') (Comarazamy, 2010; Liu et al., 2020; Zhou et al., 2020). Areas affected by heat islands have higher mean temperatures throughout the year than surrounding vegetated areas, and when wind flow is weak, heating impacts may prevail through the night with differences of as much as 12 °C between built-up and adjoining natural areas (Dai, MichelGuldmann, & Hu, 2018; Oke, 1987).

UHI are influenced by several factors including the areal extent of built-up areas (YuShih, Ahmad, Chen, PingLin, & Mabon, 2020), building density and architecture (Lima, Scalco, & Lamberts, 2019), the spatial distribution/volume of urban land uses (e.g. open/vegetated spaces: Mabon, Kondo, Kanekiyo, Hayabuchi, & Yamaguchi, 2019), and human lifestyles (e.g. preferred modes of travel: private vehicle, train, bicycle, walking, mass migration into or out of urban regions: Zhang, Wu, Yuan, Dou, & Miao, 2015; Aggarwal, 2017; Newman, 2020). Abnormally hot urban conditions may cause significant

* Corresponding author.
E-mail address: ghr.roshan@gu.ac.ir (G. Roshan).

https://doi.org/10.1016/j.scs.2021.103263
Received 28 May 2021; Received in revised form 28 July 2021; Accepted 11 August 2021
Available online 14 August 2021
2210-6707/© 2021 Elsevier Ltd. All rights reserved.

socio-environmental issues in some urban areas (Li, Sun, Li, & Gao, 2020). For instance, the number of working hours per year due to extreme hot urban conditions in southeast Asia has apparently decreased by about 10–15%; this impact is expected to double by 2050 (Kjellstorm & Meng, 2016). Rising urban temperatures and associated air pollution have adverse effects on human health and cause discomfort, with particular impacts on asthma and various respiratory diseases, as also increasing the occurrence of heatstroke, fatigue and even death (US Environmental Protection Agency, 2008).

UHI may be temporarily impacted by large-scale human activities or events, particularly through increased/decreased traffic volumes and/or particular industrial outputs associated with such activities (Imai & Yamamoto, 2015; Zhu, Wong, Guilbert, & Chan, 2017; Kamruzzaman et al., 2018; InácioPortela et al., 2020). An example is the mass out-migration of Beijing residents during the annual Chinese New Year holiday, which has led to urban temperature reductions of between 0.45 °C and 0.83 °C when compared to a 'background period' (Wu & Zhang, 2018; Zhang et al., 2015). The recent Severe Acute Respiratory Syndrome-Corona Virus Disease (COVID-19) has seen some of the largest reductions in urban activities (vehicular and air traffic, industrial outputs) at a global scale during recent times. Some environmental consequences of this have already been documented, such as improved urban and regional air quality (e.g. Ali et al., 2021; Alqasemi, Hereher, Kaplan, Fadhil Al-Quraishi, & Saibi, 2021; Chen, Hao, Zhang, & Chen, 2020; Rodríguez-Urrego & Rodríguez-Urrego, 2020; Beria et al., 2021; Kumar et al., 2021), including also over Iran (Nemati, Ebrahimi, & Nemati, 2020) and across a composite of 21 major cities in the Middle East (Kenawy et al., 2021). For instance, in Delhi (India), urban air quality improved by between 40 and 50% after only 4 days of commenced lockdown (Mahato, Pal, & Ghosh, 2020). In China, industrial lockdowns due to COVID-19 caused notable declines in NO_2 and carbon emissions (by 30 and 25% respectively: Isaifan, 2020), while in Morocco, pollutants PM_{10}, SO_2 and NO_2 declined by 75, 49 and 96% respectively (Otmani et al., 2020). In a similar study, PM_{10}, NO_2, SO_2 and CO values had declined by 45, 51, 31 and 19% respectively within a month of lockdown over Barcelona, Spain (Tobías et al., 2020). Apart from air quality, studies have now also demonstrated mean land surface temperature declines associated with lockdowns, such as for Kolkata, India (Sahani, Goswami, & Saha, 2020). Although several studies have alluded to UHI being affected through cooling associated with reduced urban activities (e.g. Ali et al., 2021; Alqasemi et al., 2021; Kenawy et al., 2021), there is a general lack of robust quantification to demonstrate such cooling effects, and that these are indeed a product of COVID-19 related urban 'lockdown' rather than regional climate-related scenarios. Although the work by Alqasemi et al. (2021) reflects on temperatures during the 2020 COVID-19 related lockdown over the United Arab Emirates, this is against temperatures of the previous year only, and thus cannot offer conclusive evidence for lockdown-related temperature reductions. A further study focusing on the city of Montreal, Canada, investigated the potential effect of COVID-19 on reducing traffic and ultimately urban heat generation (Teufel et al., 2021). The simulation approach used the limited-area version of the Global Environmental Multiscale (GEM) model, which spanned the periods January-May 2020 and April 2019-May 2020, and applied to normal and reduced traffic volumes. The key outcome of Teufel et al.'s (2021) work calculates that an 80% reduction in traffic volume equates to ~1 °C reduction in near-surface temperature. A limitation with this particular study is that it does not consider the role of synoptic climate drivers that too would influence heat generation and affect such results. Changes in UHI have also been investigated for the Indo-Gangetic Basin over the period 1 April to 15 May 2020, in comparison with the previous five years (2015–2019)(Chakraborty, Sarangi, & Lee, 2021). In this case, a combination of satellite and reanalysis products were used to establish surface energy budgets. Their results indicate >10% reduction in columnar air pollution and ~30% greater cloud cover in 2020, ultimately yielding little change in available thermal energy at the surface.

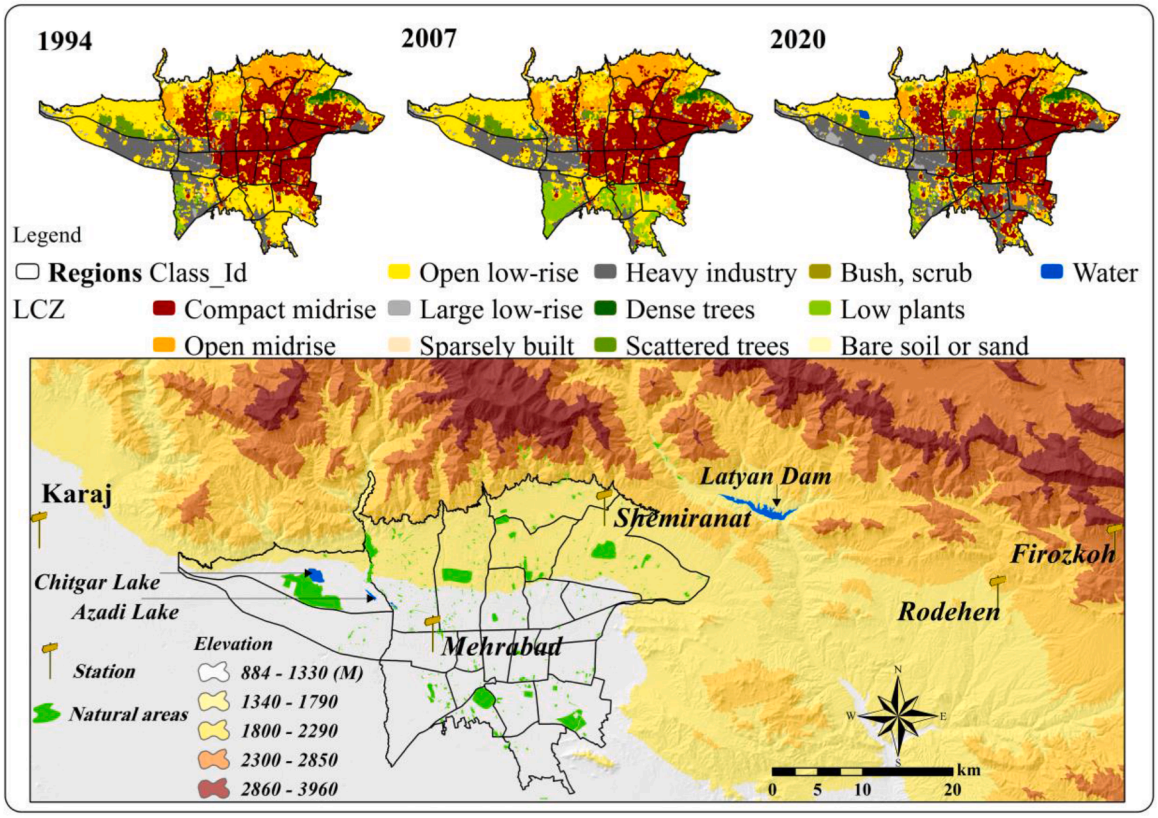

Fig. 1. Study region indicating land use changes through time and primary weather stations used in this paper.

While such studies offer valuable insight to potential thermal effects associated with reduced urban human activities, there has, as yet, not been an investigative approach using *real* station-based urban temperature data for the period of lockdown and comparing these against longer-term values. To this end, and with such a research gap in mind, we aim to establish characteristics of Tehran's urban heat island and how it was impacted through COVID-19 related 'urban lockdown'.

COVID-19 was officially declared a pandemic in Iran on 20 February 2020. This subsequently led to a nationwide lockdown to limit the spread of the disease. The lockdown commenced between 20 March and 20 April 2020, coinciding with the month of *Farvardin* (an Iranian month), which is a holiday period in Iran. The Tehran Traffic Police Control centre presented a report on vehicular traffic in the capital city, according to which traffic had decreased by ~50% by 27 February 2020 (TPTCC, 2020). Over the period 5–19 March 2020, traffic volume declined by ~70% over that for the same period in 2019. Then, from 20 March to 20 April, this downward trend continued, such that traffic volume declined by ~85% over that for the same period in 2019 (TPTCC, 2020). Given such confirmed reduced human activity over a relatively prolonged time in Tehran city, we anticipate this may have had an impact on the urban heat island, in a similar way to that reported for Beijing during the Chinese New Year, as mentioned earlier. We thus test this hypothesis and present its outcomes in the context of it being the first study to establish the indirect effects of a global pandemic on urban thermal conditions.

2. Tehran study region

Tehran metropolis covers an area of 18,909 km^2 and is located in the northern portion of the central Iranian plateau (35°07′ N; 51°24′ E). Tehran's population has seen steady growth over the last few decades and is currently estimated at ~8.3 million (Dadashpoor and Alidadi, 2017). The semi-arid climate is continental in character but with a Mediterranean-type precipitation pattern (Köppen climate classification: BSk). Geographic location has a strong influence on Tehran's climate given its proximity to the Alborz Mountains to the north, from which it receives cold and subsiding airflow. Summers are generally hot and dry (mean temp. = 28.8 °C), spring and autumn mild and relatively dry (mean spring temp. = 22.6 °C; mean autumn temp. =11.9 °C), and winters cold and wet (mean temp. = 6.8 °C) (Roshan, Shahraki, Sauri, & Borna, 2010; Ghanghermeh et al., 2013; Roshan, 2020).

3. Materials and methods

Temperature data were obtained from 1951 onwards and include the Mehrabad station in Tehran (51°19′E; 35°41′N; 1191 m asl). This station is located at Mehrabad Airport, well within the inner city region of Tehran and ~8 km from the city periphery. Temperature variables include T_{mean}, T_{max} and T_{min} and cover the period 1951–2020.

We confirm very few temperature data gaps (<1%) for all parameters (T_{mean}, T_{max}, T_{min}). Despite this, where few gaps do occur, we undertook data imputation through linear regression techniques using neighbouring station data, as per the recommendations by Valipour (2012, 2017) and Valipour, Banihabib, and Behbahani (2013). Homogeneous time series of meteorological variables are necessary for climate studies such as the one presented here. To this end, homogeneity of monthly temperature data was undertaken using the standard normal homogeneity test at the 5% significance level, following Arikan and Kahya (2019). According to the homogeneity test results, the time series of temperature (T_{mean}, T_{max}, T_{min}) for Mehrabad station have homogeneity at a 5% significance level.

For the annual time period of 20 March to 20 April, we also compare temperatures between Mehrabad station and four additional stations: Shemiranat, Karaj, Rodehen and Firozkoh (Fig. 1). For the purpose of analysis, we use the reference period 1991–2020, which represents common data availability across all four stations.

Table 1
Selected indices for analysis of extreme temperature in Iran (after Rahimzadeh, Asgari, & Fattahi, 2009).

index	Definition	Unit
SU25	Summer days: Annual count when TX (daily maximum) >25 °C	Days
TX90p	Warm days: Percentage of days when TX >90th percentile	Days
TN90p	Warm nights: Percentage of days when TN (daily minimum) >90th percentile	Days
TX10p	Cool days: Percentage of days when TX <10th percentile	Days
TN10p	Cool nights: Percentage of days when TN <10th percentile	Days
TM95p	Percentage of days when TM (mean daily) >90th percentile	Days

3.1. Evaluating temperature extremes

The World Meteorological Organization (WMO) has recommended 16 temperature extreme indicators to evaluate the effects of climate change, of which we use six as indicated in Table 1. Other indicators are not included as they are not relevant to our temporal scale of investigation. It should be noted that only the frequencies for the SU25 index have been calculated, while for other indicators, the occurrence threshold of temperature indices have been determined. Given the importance of the last two decades with respect to accelerated global warming, only these indicators are determined for the 2000s and 2010s.

3.2. Production of urban land use map

Physical development and climate change are, in combination, responsible for UHI and significant temperature differences between [some] cities and surrounding areas. However, the urban thermal layer is not uniform and fluctuates both spatially and temporally. Fluctuations (variability) in the urban thermal layer, which can be measured in near-surface air cover, vary according to the type of land use/cover and human activities. To this end, the diversity and variable intensity of human activities across the landscape have created variable microclimates within the urban environment. The process of classifying satellite images and producing thematic maps, including land use maps, and separating the city from more open/barren surrounding lands, has its challenges and is subject to subtle errors. However, in recent years, a standard and widely used method known as 'Local Climate Zone' (LCZ) classification has been established to overcome some of these challenges (e.g. Daramola & Balogun, 2019; He, Zhang, Gu, & Su, 2019; Kotharkar & Bagade, 2018). The LCZ classification strategy defines and provides all valid standards in the field of urban classification using satellite images. The LCZ algorithm, based on the climate of local zones, separates different climatic zones that exist within the bounds of the city. The standards presented in this method are globally uniform and thus do not change across regions. According to such standards provided for estimating land use changes for 17 urban classes (including various coatings of buildings with different densities and floors, along with industrial use and natural and agricultural coatings), Landsat 8 and 5 satellite images were used in the SAGA-GIS software environment (Table 2).

For Landsat 8 satellite images, 9 bands (9–10, 1 to 7) with cloud cover <10% were used, and for Landsat 5 images, bands of red, green, blue and thermal were used. The presence of thermal bands permits the separation of land uses based on temperature anomalies and microclimates. Given the nature of classes used in this method, access to terrestrial data is required. While data for some classes may be manually retrieved using Google Earth, other data, such as for residential (including the number of floors in each area of Tehran) and industrial areas, required field surveys. Such statistics are prepared by the Tehran Municipality in the form of block statistics, and are available as shape files. For more details on this method and definitions of different LCZ classes, please refer to Stewart, Oke, and Scott Krayenhoff (2014). To analyse LCZ for Tehran, three study periods (1994, 2007 and 2020) are considered, and the transformation of different classes established over these periods (Fig. 1).

Table 2
The 'Local Climate Zone' (LCZ) classification scheme and its 17 standard classes (after Stewart & Oke, 2012; Stewart et al., 2014).

Built types	Built types	Land cover types	Land cover types
1. Compact high-rise	6. Open low-rise	A. Dense trees	F. Bare soil or sand
2. Compact midrise	7. Lightweight low-rise	B. Scattered trees	G. Water
3. Compact low-rise	8. Large low-rise	C. Bush, scrub	
4. Open high-rise	9. Sparsely built	D. Low plants	
5. Open midrise	10. Heavy industry	E. Bare rock or paved	

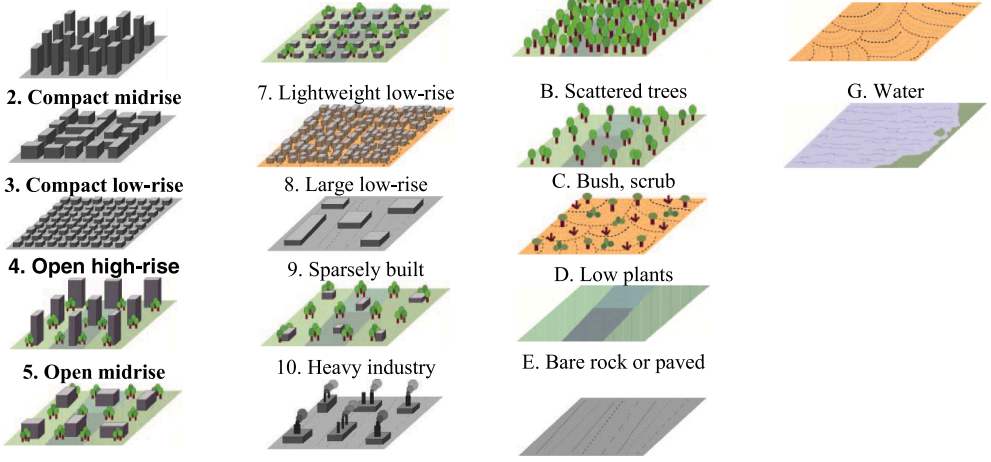

3.3. Remote sensing data analysis for establishing Tehran's urban heat island

To establish an UHI, station-based air temperature data are required, for which Modis (Moderate Resolution Imaging Spectroradiometer) Terra satellite (originally known as EOS AM-1) data were used as 8-day composite images. The advantage of applying 8-day rather than daily data, is that these images have less cloud cover and thus least amount of lost information in each frame. Modis, with code MOD11A2, was programmed and coded from Google EarthEngine website of Terra satellite images. This product (MOD11A2) is a temperature indicator with a spatial resolution of 1000 m and time-frame of 8 accumulated days, covering the period of 20 March to 20 April for each year from 2000 to 2020. To complete and implement a spatial analysis of temperature, the Spatial Statistics Tools section of Mapping Clusters subset (Getis-Ord Gi) Hot Spot Analysis was used in the Arc GIS software.

Hot Spot Analysis entails calculating the Getis-Ord G_i^* statistic for air temperature in context with neighbouring cell temperatures. The G_i^* value is a z-score indicating where high or low values are clustered. For a hot spot to be statistically significant, a given location will have a high value, and is surrounded by high values. The Getis-Ord statistic is calculated according to the formula (ESRI, 2018):

$$G_i^* = \frac{\sum_{j=1}^{n} W_{i,j} - x\sum_{j=1}^{n} W_{i,j}}{s\sqrt{\frac{n\sum_{j=1}^{n} W_{i,j}^2 - \left(\sum_{j=1}^{n} W_{i,j}\right)^2}{n-1}}} \quad (1)$$

Where i is the resultant G_i^* statistics (z-scores and p- values) for pixel i, xj is the LST value for pixel j, wi,j is the spatial weight between pixel i and neighbouring pixel j, n is equal to the total number of pixels, and $\overline{X}$ and S are mean and variance:

$$\overline{X} = \frac{\sum_{j=1}^{n} x_j}{n} \quad (2)$$

and

$$S = \sqrt{\frac{\sum_{j=1}^{n} x_j^2}{n} - \left(\overline{X}\right)^2} \quad (3)$$

Table 3
Classification based on p value and z score (Georgiana & Uritescu, 2018).

Significance level (p value)	Critical Value (z-score)	Class No	Class name
-0.01	<-2.58	1	Very cold spot
-0.05	-2.58 to -1.96 2	2	Cold spot
-0.10	-1.96 to -1.65	3	Cool Spot
0	0 -1.65 to 1.65	4	Not significant
0.10	1.65 to 1.96	5	Warm spot
0.05	1.96 to 2.58	6	Hot spot
0.01	> 2.98	7	Very hot spot

The G_i^* statistic (z-score) output represents the statistical significance of clustering for a specified distance (ESRI, 2018). The z-score was then compared with a range of values entailing seven confidence levels (Table 3): -0.01 (values < -2.58); -0.05 (values ranging from -2.58 to -1.96); -0.1 (values ranging from -1.96 to -1.65); 0 (values ranging from -1.65 to1.65); 0.1 (values ranging from 1.65 to 1.96); 0.05 (values ranging from 1.96 to 2.58); and 0.01 (values > 2.98). The seven levels correspond to seven classes that LST values were assigned to. These are most important for analysing "very cold spots" and "very hot spots", which define areas with extreme values.

The MOD11A2 V6 product provides an average 8-day land surface temperature (LST) in a 1200 × 1200 km grid. Each pixel value in MOD11A2 is a simple average of all the corresponding MOD11A1 LST pixels collected over the given 8-day period. The 8-day compositing period was chosen, given that double this period represents the exact ground track repeat period of the Terra and Aqua platforms. Along with both the day- and night-time surface temperature bands and their quality indicator (QC) layers, are also MODIS bands 31 and 32 and eight observation layers (https://doi.org/10.5067/MODIS/MOD11A2.006). The specifications for each of the images was obtained from the Google Earth Engine system, related to the Terra satellite Modis sensor. All downloaded images are for the period 20 March to 20 April for each year (2000–2020), with Kelvin evaluation unit, numerical range of 7500 to 65,535, scale factor of two hundredths, pixel size of 100 m, 16-bit data type, and 8-day time separation. The urban heat island analysis programming can be viewed inside the Google EarthEngine website through the following link.

Uhi Code.Rtf

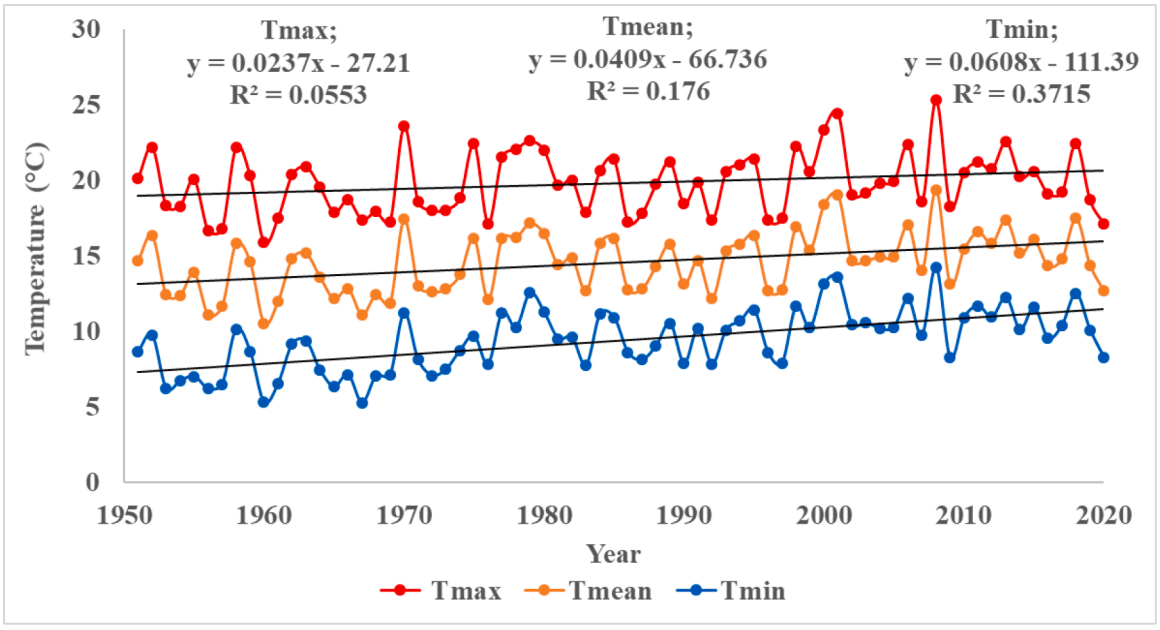

Fig. 2. Mean T_{mean}, T_{max} and T_{min} (°C) for Tehran over the period 20 March to 20 April each year: 1951–2020.

https://code.earthengine.google.com/?scriptPath=users%2Fsarlireza839%2Fexample_1%3AThermal%20Island

3.4. Synoptic evaluation of temperature changes at 500 and 700 hPa levels

As already alluded to, UHI intensity may be affected by a variety of urban parameters such as transport type and volume, land use change, density of buildings, etc., or by atmospheric systems affecting it. To this end, we assess the potential role of atmospheric and synoptic systems controlling the UHI over Tehran. Although various synoptic indicators may be used to address this, the function of all indicators is to establish how synoptic patterns in the study area might increase or decrease urban temperatures. Hence, in our final product, we determine the variability of spatio-temporal patterns of temperature at high atmospheric levels. To achieve this, temperature data at two atmospheric levels (500 and 700 hPa) are used. Mean temperatures for the desired levels are established for a latitudinal range of 37.5° to 35°N and longitudinal range of 50.0° to 52.5°E, which includes the city of Tehran and four additional cities selected for this study. Data and analysis are specifically for the period of 20 March to 20 April each year, over the years 1950–2020. Daily data were obtained from the NCEP/NCAR Extract site and mean values prepared for each period according to coding in the environment Grads.

3.5. Classification and regression trees (CART) for establishing areal changes in the urban heat island

Classification and regression trees (CART) is a computable algorithm used for data mining (Breiman, Friedman, Olshen, & Stone, 1984). Constructed trees assist in the prediction (regression tree) and classification (classification tree) of new observations. While classification trees are based on dependent variables, regression trees do not have predefined classes. The CART methodology includes the construction of maximum trees, choice of most suitable tree size and the classification or production of new data using the constructed tree. Here we use CART to predict the areal extent (hectares) of daytime UHI depicted through temperature of atmospheric systems at 500hPa and 700hPa levels. The first step involves the splitting and construction of maximum trees, which is based on the squared residuals minimization algorithm. Pruning techniques and cross-validation procedures are applied according to Timofeev (2004). By increasing tree size (i.e. tree complexity), misclassification errors are reduced. The complexity parameter (cp) was then used to select the optimal decision tree size, which was identified through trial and error. When the regression tree is constructed, it provides a specific response value to each of the new observations. In order to validate the modelled results, some performance criteria are required; these include: a) the Nash–Sutcliffe efficiency (NSE) coefficient (Nash & Sutcliffe, 1970) (Eq. (4)), b) the ratio of the root mean square error (RMSE) to the standard deviation of measured data (RSR) (Eq. (5))(Choubin et al., 2018) and c) the coefficient of determination (R2).

$$NSE = 1 - \frac{\sum_{i=1}^{N}(O_i - P_i)^2}{\sum_{i=1}^{N}\left(O_i - \overline{O}\right)^2} \tag{4}$$

$$RSR = \frac{RMSE}{STDEV_{obs}} = \frac{\left[\sqrt{\sum_{i=1}^{N}(O_i - P_i)^2}\right]}{\left[\sqrt{\sum_{i=1}^{N}\left(O_i - \overline{O}\right)^2}\right]} \tag{5}$$

Where N is the number of data points, O_i and P_i are the observed and predicted ith values, $\overline{O}$ is the mean of the observed values.

4. Results and discussion

4.1. Long-term temperature changes for Tehran

T_{mean} for the period 20 March to 20 April over the years 1951 to 2020 is 14.54 °C (Fig. 2). The period 1960–1969 is considerably cooler (av = 12.60 °C) than times since (1961–2020; av = 14.74 °C). The most recent couple of decades (2000–2020) are distinctly warmest (av = 15.72 °C). For the year 2020, T_{mean} is 12.67 °C, and thus represents a significant negative temperature departure from the multi-decadal mean (-1.86 °C), but even more so from the mean of the last two decades (-3.00 °C). This also represents the lowest T_{mean} for this annual time-period since 1992 (i.e. last 29 years).

Mean T_{max} for the period 20 March to 20 April over the years 1951 to 2020 is 19.81 °C (Fig. 2). As was the case for T_{mean}, the period 1960–1969 is considerably cooler (av = 18.32 °C) than times since

Table 4
Mean T_{mean}, T_{max} and T_{min} (°C) for five weather stations over the period 20 March to 20 April: 1994–2020.

Mean(1991–2020)				2020			T departure		
Stations	T_{mean}	T_{max}	T_{min}	T_{mean}	T_{max}	T_{min}	T_{mean}	T_{max}	T_{min}
Mehrabad	15.6	20.4	10.8	12.7	17.0	8.2	-2.9	-3.3	-2.5
Shemiranat	13.2	18.2	8.2	10.8	15.3	6.2	-2.4	-2.8	-2.0
Karaj	13.5	18.7	7.0	10.5	15.6	5.3	-2.9	-3.0	-1.7
Rodehen	5.4	9.6	1.1	3.4	7.2	-0.3	-1.9	-2.4	-1.5
Firozkoh	6.9	13.9	-0.1	5.3	11.5	-0.8	-1.5	-2.3	-0.7

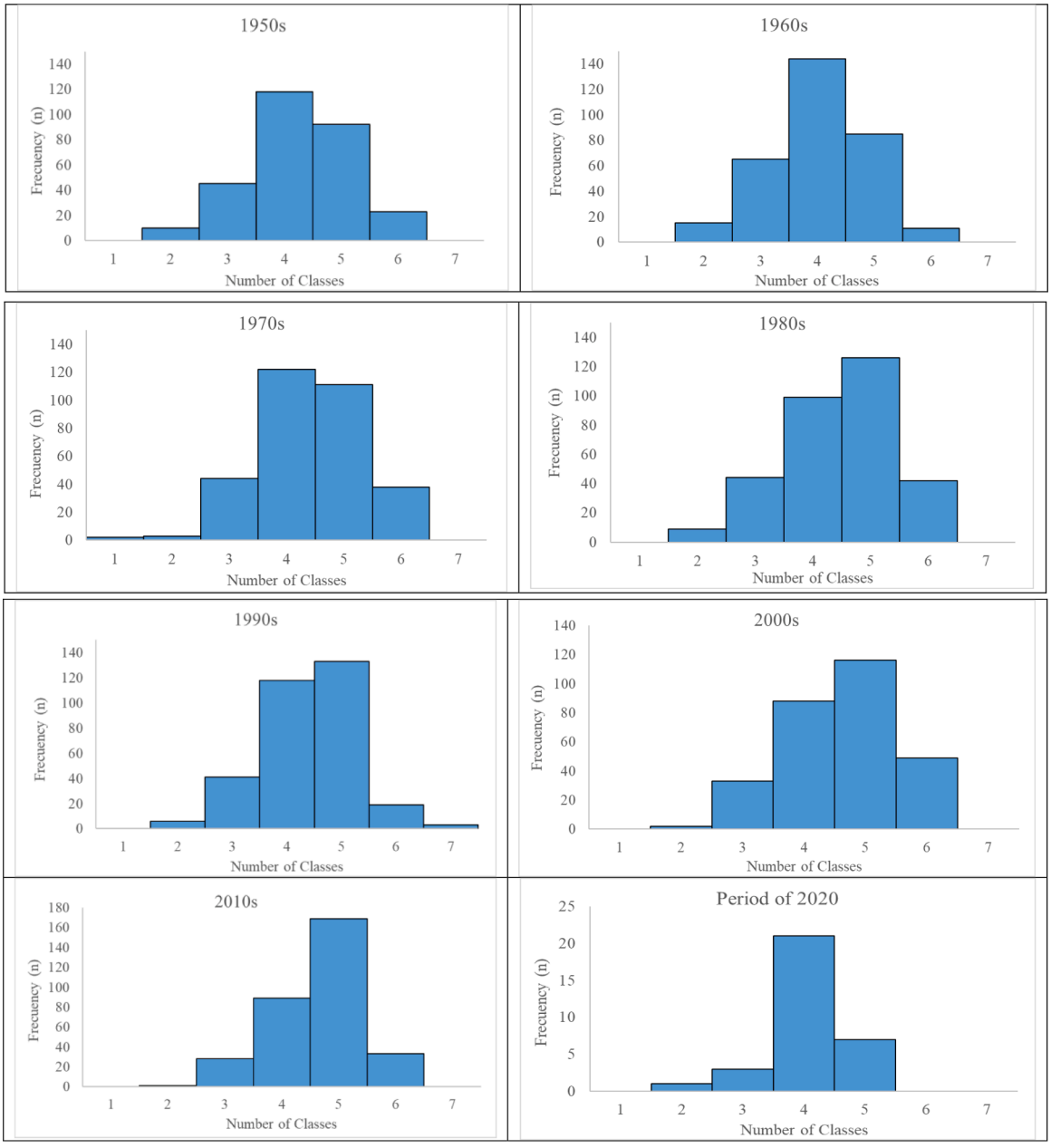

Fig. 3. Mean frequency of daily temperature threshold classes for Mehrabad weather stations over the period 20 March to 20 April. Data are for the late 20th and early 21st centuries, and for the year 2020.

(1961–2020) then (av = 19.93 °C). The most recent couple of decades (2000–2020) are distinctly warmest (av = 20.60 °C). This warming trend may in part, be attributed to urban expansion and associated human-induced warming factors. For the year 2020, mean T_{max} is 17.09 °C, and thus represents a significant negative temperature departure from the multi-decadal mean (-2.72 °C), but even more so from the mean of the last two decades (-3.50 °C). This also represents the lowest mean T_{max} for this annual time-period since 1960 (i.e. last 60 years).

Mean T_{min} for the period 20 March to 20 April over the years 1951 to 2020 is 9.4 °C (Fig. 2). The period 1950–1980 is considerably cooler (av = 8.20 °C) than times since then (av = 10.30 °C). The most recent couple

Table 5
Frequency of temperature occurrence for different temperature classes.

Number of Classes	1	2	3	4	5	6	7
class of Temperature(°C)	<0	0.1–5	5.1–10	10.1–15	15.1–20	20.1–25	<25
2000	0	0	0	5	**15**	11	1
2001	0	0	1	2	**17**	12	0
2002	0	0	4	12	**15**	1	0
2003	0	0	6	**14**	6	6	0
2004	0	1	4	10	**12**	5	0
2005	0	1	6	8	**12**	5	0
2006	0	0	0	11	**16**	5	0
2007	0	0	8	10	**12**	2	0
2008	0	0	0	1	**18**	13	0
2009	0	0	4	**20**	8	0	0
2010	0	0	4	8	**19**	1	0
2011	0	0	1	10	**18**	3	0
2012	0	0	1	12	**15**	4	0
2013	0	0	0	7	**19**	6	0
2014	0	0	7	6	**14**	5	0
2015	0	0	2	9	**18**	3	0
2016	0	0	3	10	**19**	0	0
2017	0	1	5	8	**15**	3	0
2018	0	0	2	6	**17**	7	0
2019	0	0	3	13	**15**	1	0
2020	0	1	3	**21**	7	0	0

of decades (2000–2020) are distinctly warmest (av = 11.00 °C). For the year 2020, the mean T_{min} is 8.24 °C, and thus represents a significant negative temperature departure from the multi-decadal mean (-1.15 °C), but even more so from the mean of the last two decades (-2.72 °C). This also represents the lowest mean T_{min} for this annual time-period since 1997 (i.e. last 23 years).

4.2. Long-term temperature changes between the five stations

The stations of Mehrabad and Shemiranat are located in Tehran city centre (inner city) and thus in the core of the UHI. The stations of Karaj (35 km), Rodehen (52 km) and Firozkoh (128 km) are located with increasing distance, respectively, from the inner Tehran city periphery, or core of the heat island (see Fig 1a). Notably, T_{max} departures for the period 20 March to 20 April in 2020 from the 1991–2020 reference period, is consistently stronger at all stations than T_{min} (Table 4). In the context of COVID-19 related lockdown and the urban heat island, these diurnal temperature departures correspond with maximum decline in human activity during the day and to a lesser extent during the night. The stations of Mehrabad (-2.89 °C), Karaj (-2.93 °C) and Shemiranat (-2.41 °C) indicate strongest mean negative temperature departures in 2020, while the two most distant stations from the city centre, namely Rodehen and Firozkoh, record comparatively weaker negative departures (-1.97 and -1.54 °C respectively), yet even these are significant. Notably, although Karaj is located 52 km beyond the inner city periphery, it is also a metropolis in the neighbourhood of Tehran, affected by the UHI. These results thus demonstrate maximum cooling effects during 2020 in the most built-up and busiest sectors of Tehran, while the cooling anomaly diminishes in strength with distance into the more outlying parts of the city where the heat island is less pronounced.

4.3. Frequency classes for daily mean temperature

Here we present daily temperature threshold classes related to the peak (frequency) of daily mean temperatures for each decade of the study (Fig 3). Seven threshold classes for daily mean temperatures during the period 20 March to 20 April each year, are represented as follows: class 1 = <0 °C, class 2 = 0.1 to 5 °C, class 3 = 5.1 to 10 °C, class 4 = 10.1 to 15 °C, class 5 = 15.1 to 20 °C, class 6 = 20.1 to 25 °C, and class 7 = >25.1 °C. Mean decadal values, as also those for the year 2020, are calculated and plotted (Fig. 3).

Two patterns of daily temperature threshold class occurrences are observed for different decades. The first pattern is from the 1950s to the 1970s, during which time the maximum frequency (peak) of daily mean temperature occurrence belongs to the fourth class (i.e. temperature threshold of 10.1 to 15 °C) and follows a normal distribution (Fig. 3). However, from the 1980s to 2010s, the peak (frequency) shifted to the fifth class (i.e. temperature threshold of 15.1 to 20 °C) and is negatively skewed. This seems a product of global/regional warming. Notably, during 2020, the peak (frequency) shifts back to the fourth class, as was the case during the 1970s and earlier, which is in strong contrast to outputs during the last two decades in particular. In fact, the class frequency distribution for 2020 is most closely aligned to that for the 1950s and 1960s.

For most years during the last two decades, the highest frequency of daily T_{mean} is situated in the fifth class with a temperature threshold of 15.1 to 20.0 °C. Years with a maximum frequency (19 events each) of daily T_{mean} in the fifth class include 2010, 2013 and 2016. In contrast, only three years have their highest frequency of daily T_{mean} in the fourth class with a temperature threshold of 10.1 to 15.0 °C; namely 2003,

Table 6
Threshold and frequency of temperature extreme indicators in Tehran over the last two decades.

Years	SU25 (days)	TX90p (C°)	TN90p (C°)	TX10p (C°)	TN10p (C°)	TM95p (C°)
2000	11	29.4	18.4	17.4	7.6	23.9
2001	15	28.6	18.8	20.0	9.0	24.1
2002	1	24.6	15.4	13.0	5.4	20.0
2003	7	28.6	19.6	13.6	5.6	24.1
2004	4	25.6	15.6	14.2	1.6	21.2
2005	4	26.2	17.0	12.4	2.2	22.5
2006	6	27.6	17.8	18.2	7.0	23.2
2007	0	24.2	15.8	12.2	3.0	20.1
2008	15	29.0	18.4	21.6	10.6	24.2
2009	0	21.6	12.6	14.0	2.0	16.6
2010	4	25.4	16.4	13.4	5.0	20.0
2011	3	26.4	16.0	17.2	7.0	22.0
2012	4	27.6	17.4	16.2	4.6	23.9
2013	6	26.0	16.4	18.4	8.6	21.6
2014	5	25.8	15.4	14.4	3.8	20.9
2015	4	26.4	16.4	14.5	6.0	22.2
2016	0	23.2	13.0	14.8	4.4	18.1
2017	3	26.0	16.2	9.6	4.0	21.9
2018	9	28.2	18.8	13.0	6.2	23.7
2019	2	23.8	14.5	12.2	6.2	19.2
2020	**0**	**22.0**	**12.8**	**9.4**	**3.6**	**17.8**

Table 7
Land use changes over Tehran: 1994–2020. Class Id's are as follows: 2= Compact midrise; 5= Open midrise; 7= Lightweight low-rise; 8= Large low-rise; 9= Sparsely built; 10= Heavy industry; 11= Dense trees; 12= Scattered trees; 13= Bush, scrub; 14= Low plants; 16= Bare soil or sand; 17= Water.

	1994			2007			2020	
Class_Id	Area (hectares)	%	Class_Id	Area (hectares)	%	Class_Id	Area (hectares)	%
2	18,459	30.13	2	18,355	29.96	2	21,161	34.54
5	9378	15.31	5	9265	15.12	5	9467	15.45
7	18,983	30.99	7	16,403	26.77	7	11,970	19.54
8	563	0.92	8	497	0.81	8	1012	1.65
9	214	0.35	9	159	0.26	9	214	0.35
10	9887	16.14	10	9755	15.92	10	13,260	21.64
11	623	1.02	11	623	1.02	11	623	1.02
12	1549	2.53	12	1544	2.52	12	1807	2.95
13	82	0.13	13	82	0.13	13	82	0.13
14	897	1.46	14	3966	6.47	14	897	1.46
16	595	0.97	16	580	0.95	16	595	0.97
17	34	0.06	17	34	0.06	17	176	0.29

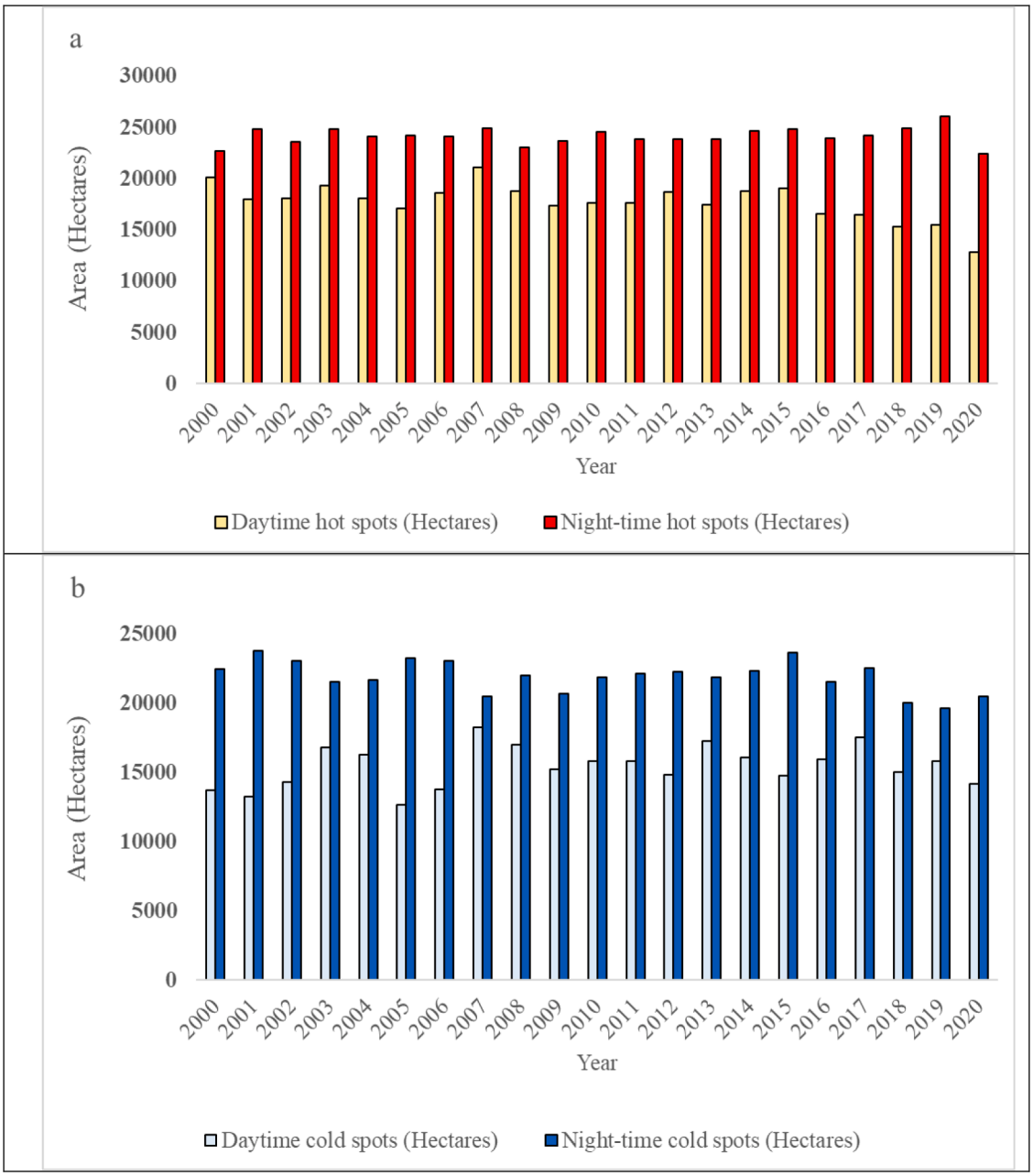

Fig. 4. Spatial coverage of annual: a) hot spots and b) cold spots for Tehran metropolis: 2000–2020.

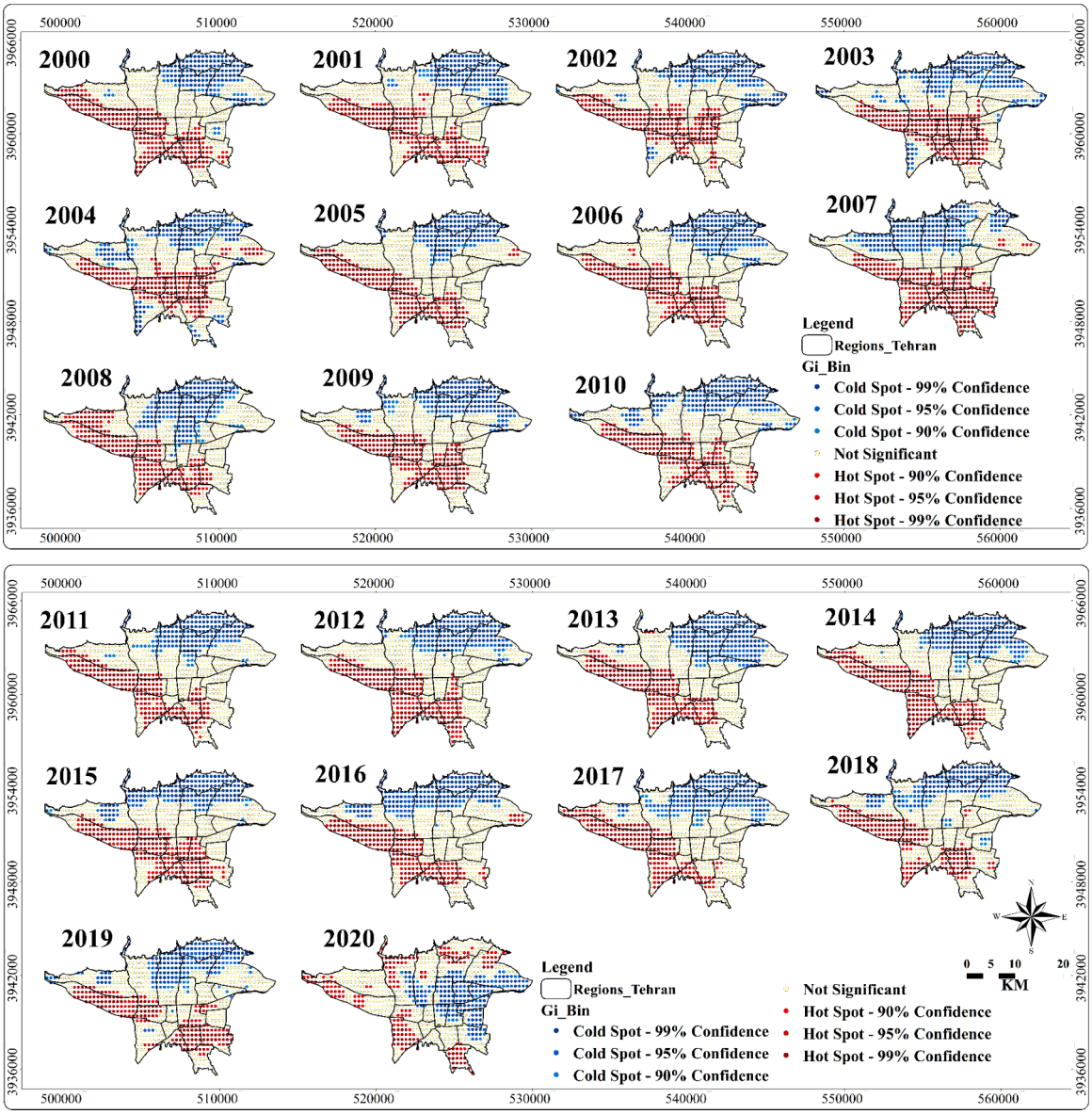

Fig. 5. Spatial pattern of heat and cold islands (daytime) for the metropolis of Tehran during the period 20 March to 20 April: 2000–2020.

2009 and 2020. Most years (18) during the last two decades have negatively skewed T_{mean} values (Table 5). However, 2020 contrasts strongly with this tendency and demonstrates a normal distribution.

4.4. Thresholds and frequency of temperature extreme indicators

Thresholds of temperature extreme indicators were determined for each year over the period 20 March to 20 April, while the frequency (in days) is indicated for the SU25 index (Table 6). Highest occurrences (15 days) for the SU25 Index are recorded in 2001 and 2008. In contrast, no incidents are recorded in four years since 2000, one of these being 2020. The threshold value for the TX90p index was particularly high over the years 2000–2008 (av = 27.10 °C) and reached a maximum value (29.40 °C) in 2000. The mean index value has been somewhat lower over the years 2009–2020 (av = 25.20 °C), with lowest values recorded in 2009 (21.60 °C) and 2020 (22.0 °C). This pattern repeats itself for the TN90p index, with the period 2000–2008 recording a mean index value of 17.40 °C, while that for 2009–2020 is 15.5 °C. A maximum threshold value of 19.6 °C is reached in 2003. Again, lowest values are for 2009 (12.6 °C) and 2020 (12.80 °C). Extreme cool daytime thresholds represented by the TX10p indicate that the lowest value in the last 20 years was recorded in 2020 (9.40 °C). The extreme cool nighttime threshold (TN10p) in 2020 (3.60 °C) is also well below the mean (5.40 °C) threshold value for the last two decades and the lowest since 2009 (2.00 °C). Finally, the 2020 value for the TM95p index is second lowest (17.80 °C) only to the 2009 (16.60 °C) value and well below the mean for the last two decades (21.50 °C). Overall, as far as extreme temperature threshold values are concerned during the last two decades, two years stand out; namely 2009 and 2020. In the case of 2009, this is due to unusual cold synoptic anomalies from the north. In the case of 2020, there were no such cold synoptic anomalies and thus we attribute the extremes in this year to COVID-19 related lockdown factors, as discussed in this paper.

4.5. Spatio-temporal land use changes over Tehran

Outputs depicting land use change over Tehran indicate that in 1994, Class 7 (lightweight low-rise) covered 30.99%, Class 2 (compact mid-rise) covered 30.13%, Class 10 (heavy industry) covered 16.14% and Class 5 (open midrise) covered 15.31% of area. All other land use types

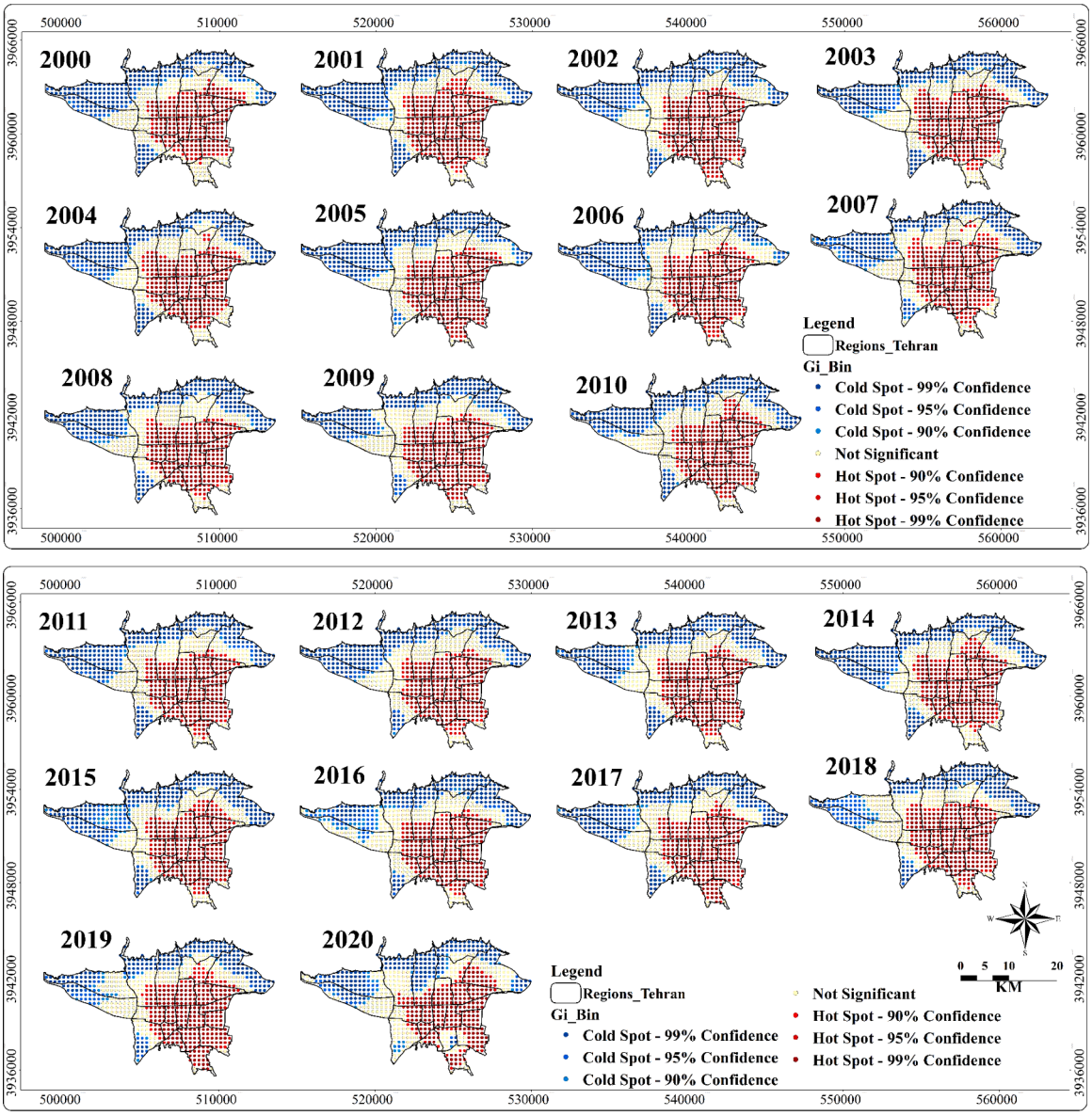

Fig. 6. Spatial pattern of heat and cold islands (night-time) for the metropolis of Tehran during the period 20 March to 20 April: 2000–2020.

over the greater Tehran Metropol made up the remaining 7.44% of area. General similarities in percentage class types are recorded for the year 2007. Although Class 7 drops to 26.77%, Classes 2, 10 and 5 remain similar at 29.96%, 15.92% and 15.12% respectively, while other land use types make up the remaining 12.22%. Possibly the most noteworthy change identified under 'other land use types' is that Class 14 (low plants) had increased in areal extent from 1.46% to 6.47% between 1994 and 2007 (Table 7). By the year 2020, Class 7 had dropped further to cover only 19.54% of area, while in contrast Classes 2 and 10 had increased considerably in area to cover 34.54 and 21.64% respectively. Notably, the expansion of heavy industrial areas (Class 10) is likely to have impacted on the formation and intensification of the UHI given that its thermal energy outputs exceed those generated by other land use classes. No significant change is measured for Class 5 between 1994 (15.31%) and 2020 (15.45%). In addition, 'other classes' (Classes 11 to 14), which represent less reflective surfaces through 'green space', are better suited to reducing the UHI effect than are more reflective surfaces. Such classes have, however, also not changed much in percentage area between 1994 (5.18%) and 2020 (5.45%).

A further class that may be very effective in reducing the UHI, but increase cold islands, is the presence of water (Class 17). Local water bodies have increased from 34 hectares in 1994 to 176 hectares in 2020, primarily due to the construction of the Chitgar Dam in 2013, and the subsequently established lake, which covers 130 hectares in extent since 2013. Fig. 1 and Table 7 indicate the distribution of different land uses over Tehran during the study period 1994–2020.

4.6. *Spatio-temporal variability of Tehran's UHI: 2000–2020*

We now focus attention on the spatio-temporal variability of Tehran's UHI (both daytime and night-time) for the period 20 March to 20 April during the last two decades (Fig. 5 and Fig. 6). For this, we use a simple linear regression test (i.e. parametric test) to determine trends. The Pearson correlation coefficient indicates the significance of such trends/changes, denoted by the symbol r, which varies between +1 and -1.

The surface area of both 'hot spots' and cold spots' are calculated for each year, as explained in the methods section. Most notable from these findings is that the year 2020 records the lowest areal extent (12,804 hectares) of daytime hot spots since the year 2000 and is considerably

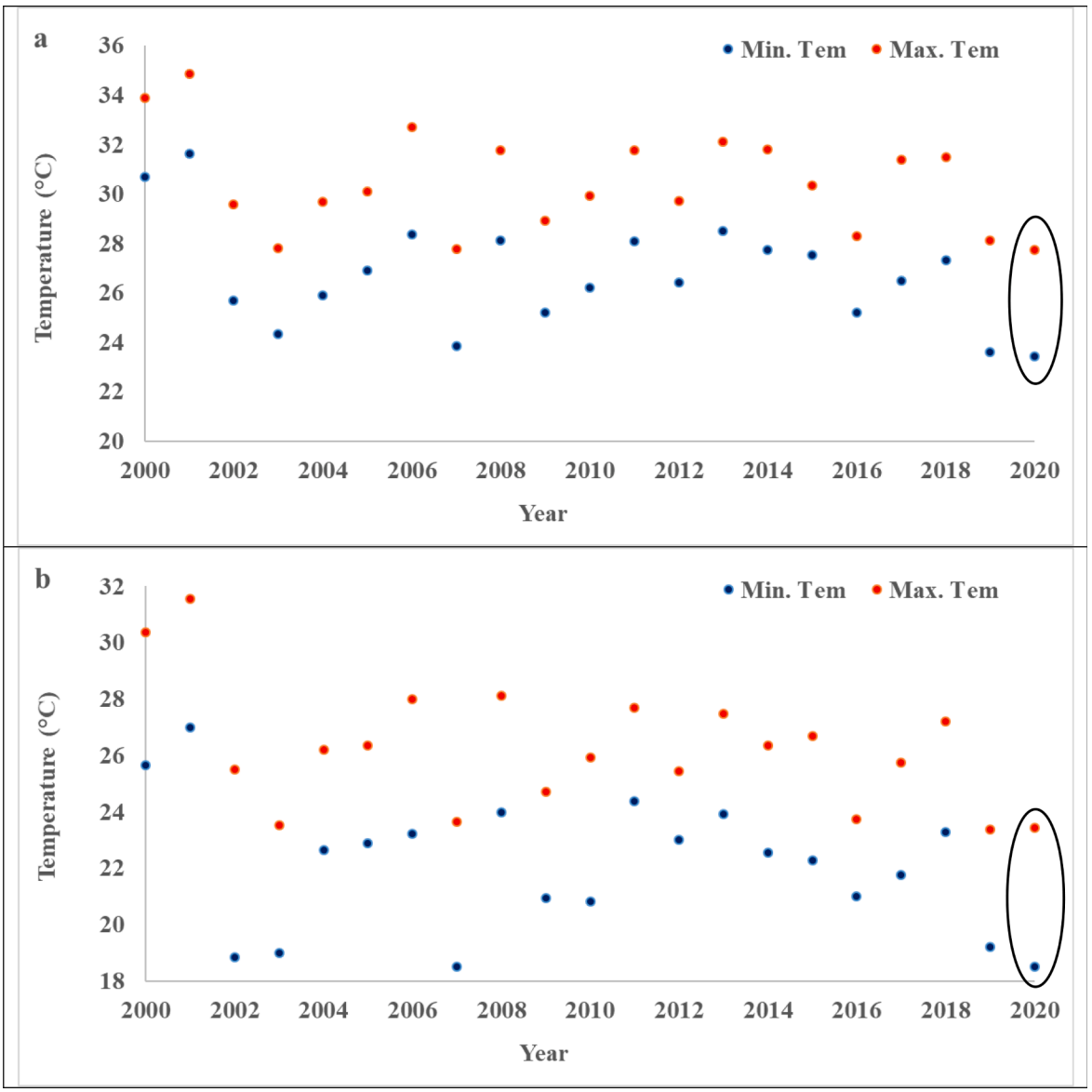

Fig. 7. T_{max} and T_{min} threshold values for daytime a) heat and b) cold islands and night-time c) heat and d) cold islands during the study period 2000–2020.

below the mean value for the last two decades (mean = 17,733 hectares), as also that for the second lowest recorded (15,303 hectares) in the year 2018 (Fig. 4a). Likewise, night-time records indicate the lowest UHI extent for 2020 (22,414 hectares), followed by the year 2000 (22,703 hectares; mean for 2000–2020 = 24,164 hectares). This indicates that the UHI over Tehran had its smallest diurnal spatial extent in 2020. A considerable overall increasing trend in the spatial extent of Tehran's UHI is recorded over the period 2000–2019 ($r = 0.41$; at the 95% significance level). However, if considered over the period 2000–2020, this trend is substantially weakened to $r = 0.15$, hence indicating the extent of 2020 as an outlier year, especially in the context of the last 20 year trend.

The spatial extent of daytime cold spots during 2020 (14,131 hectares) is not as extensive as might have been expected, and in fact is marginally below the 2000–2020 mean (by 1298 hectares) (Fig. 4b). The spatial extent of night-time cold spots in 2020 (20,459 hectares) is also somewhat lower than the mean for the period 2000–2020 (21,893 hectares). This is perhaps to be expected given the strong overall spatial decline in cold islands ($r = -0.5$) between 2000 and 2020.

Fig. 5 presents the annual spatial distribution of daytime urban heat/cold islands across the metropolis of Tehran for the period 20 March to 20 April since 2000. Heat islands are most prominent over western and southern portions of the metropolis. Noteworthy is a spatially-continuous strip of heat island extending from the western city periphery to southeastern periphery over the years 2000–2017. However, during the last three years (2018–2020), this elongated heat island seems to have become fragmented in easternmost regions, and is hence becoming spatially-discontinuous.

Some notable spatial differences in both heat and cold islands occur in 2020, which contrasts strongly to all other years. In the first instance, large spatially-continuous heat islands are not present in 2020, but rather occur as 'small pockets' of heat islands. This most likely reflects a displacement of areas which usually encounter maximum human movement\activity (i.e. areas of work [industrial outputs, transport hubs etc.], school or university attendance) to peripheral areas of residence – a situation rather unique to 2020 given the COVID-19 related lockdown, which may account for the patchy 'heat pockets'. Secondly, the northernmost sector of the metropolis in all previous years was characterized by a large cold island, yet for the first time since 2000, this part of the city experienced small pockets of heat islands. This may be

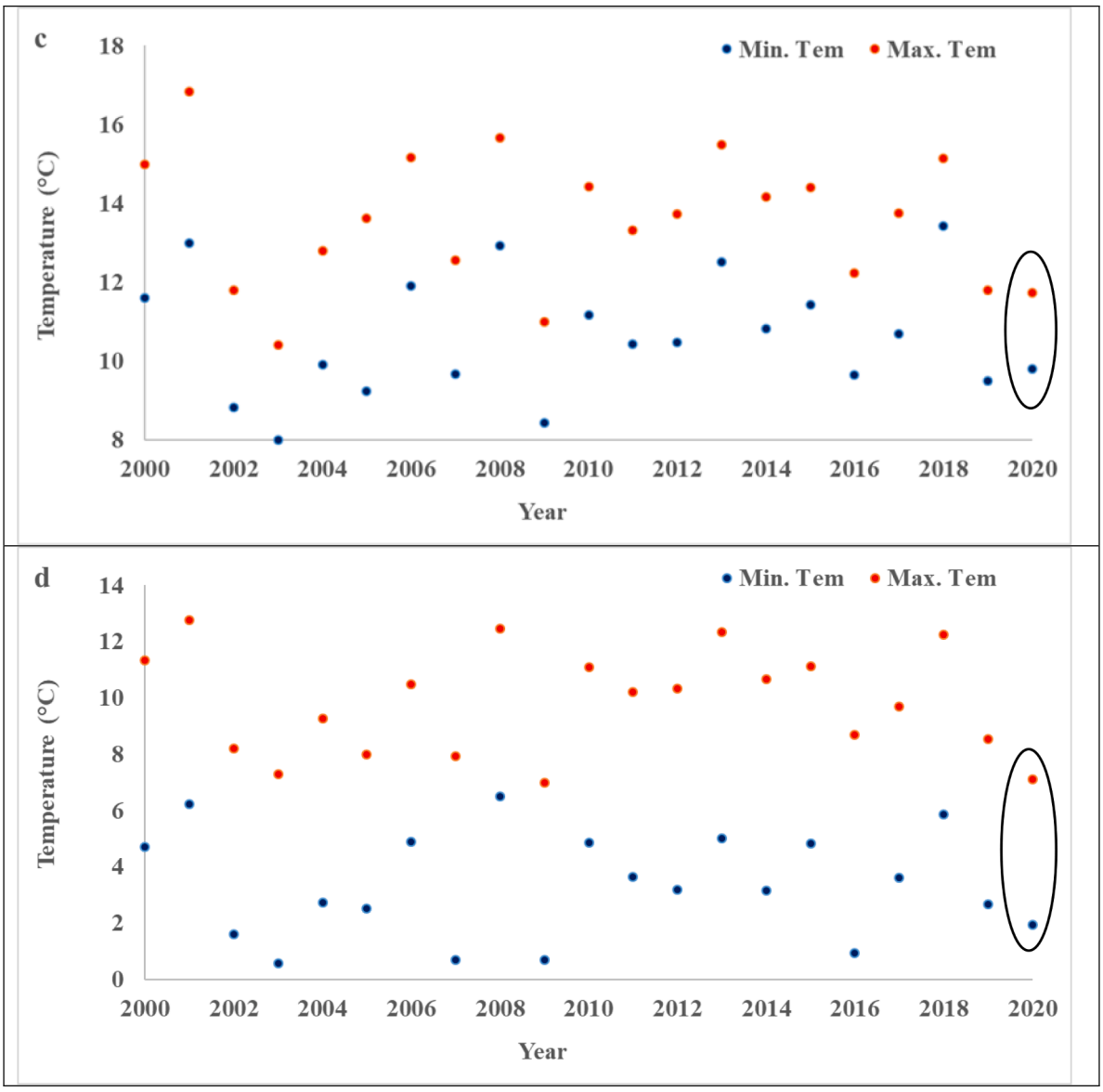

Fig. 7. (*continued*).

due to this being a densely populated residential area to which many would have been restricted during the lock-down, and hence may be associated with enhanced (above normal) residential heating outputs in 2020. Thirdly, for the first time since 2000, the entire central to eastern portion of the metropolis experienced a large cold island, which is typically a busy transport route and industrial output region of the city, but which would have been largely 'shut-down' during the period 20 March to 20 April of 2020. In essence then, what would usually have been a cold island over the northern metropolis, has been displaced by a heat island, and instead a cold island has established itself over central-eastern portions of the city.

We now present mean T_{max} and T_{min} for heat and cold islands as depicted in Fig. 7. Findings show that mean T_{max} and T_{min} values for daytime heat islands over the period 20 March to 20 April each year from 2000 to 2020 is 30.5 °C and 26.7 °C respectively (Fig. 7a). Accordingly, both mean T_{max} and T_{min} values are lowest (27.75 °C and 23.43 °C respectively) for the year 2020. Similarly, mean T_{max} and T_{min} for cold islands are also lowest in 2020 (23.45 °C and 18.55 °C respectively), although T_{max} is similar to that recorded in 2019 (23.38 °C) and T_{min} similar to that in 2007 (18.51 °C)(Fig. 7b). Mean T_{max}/T_{min} values for cold islands are 26.30 °C and 22.00 °C respectively for the full period 2000–2020. Night-time UHI temperature threshold values in 2020 (mean T_{max} = 11.73 °C; T_{min} = 9.8 °C) are somewhat higher than the longer-term mean for the period 2000–2020 (mean T_{max} = 13.58 °C; T_{min} = 10.64 °C). The same applies for night-time cold islands in 2020 (mean T_{max} = 7.12 °C; T_{min} = 1.95 °C; mean for the period 2000–2020: T_{max} = 9.85 °C; T_{min} = 3.38 °C).

Six temperature classes were established for both daytime and night-time, based on absolute maximum and minimum values for each of these diurnal periods. Over the period 20 March to 20 April 2000 to 2020, daytime temperatures varied from a minimum of 18.5 °C in 2007 to a maximum at 34.9 °C in 2001. Based on these extreme outliers, we provide six temperature classes as shown in Fig. 8. The greatest areal extent (10% of Tehran) of the coldest temperature class (18 to 20.9 °C) occurred in 2007. However, the greatest extent (74.2% of Tehran) of the two coldest temperature classes (18 to 23.9 °C) occurred in 2020. Interestingly, although there were large areal extents of cold islands in years such as 2008 and 2013, these do not record any area of the city reaching the two coldest temperature class values. Although the largest extent of the UHI occurred in 2007 (21,120 hectares), no area of the city experienced the most extreme heat classes (30 to 35.9 °C) that year. Largest areal extent of extreme heat (30 to 35.9 °C) was recorded in

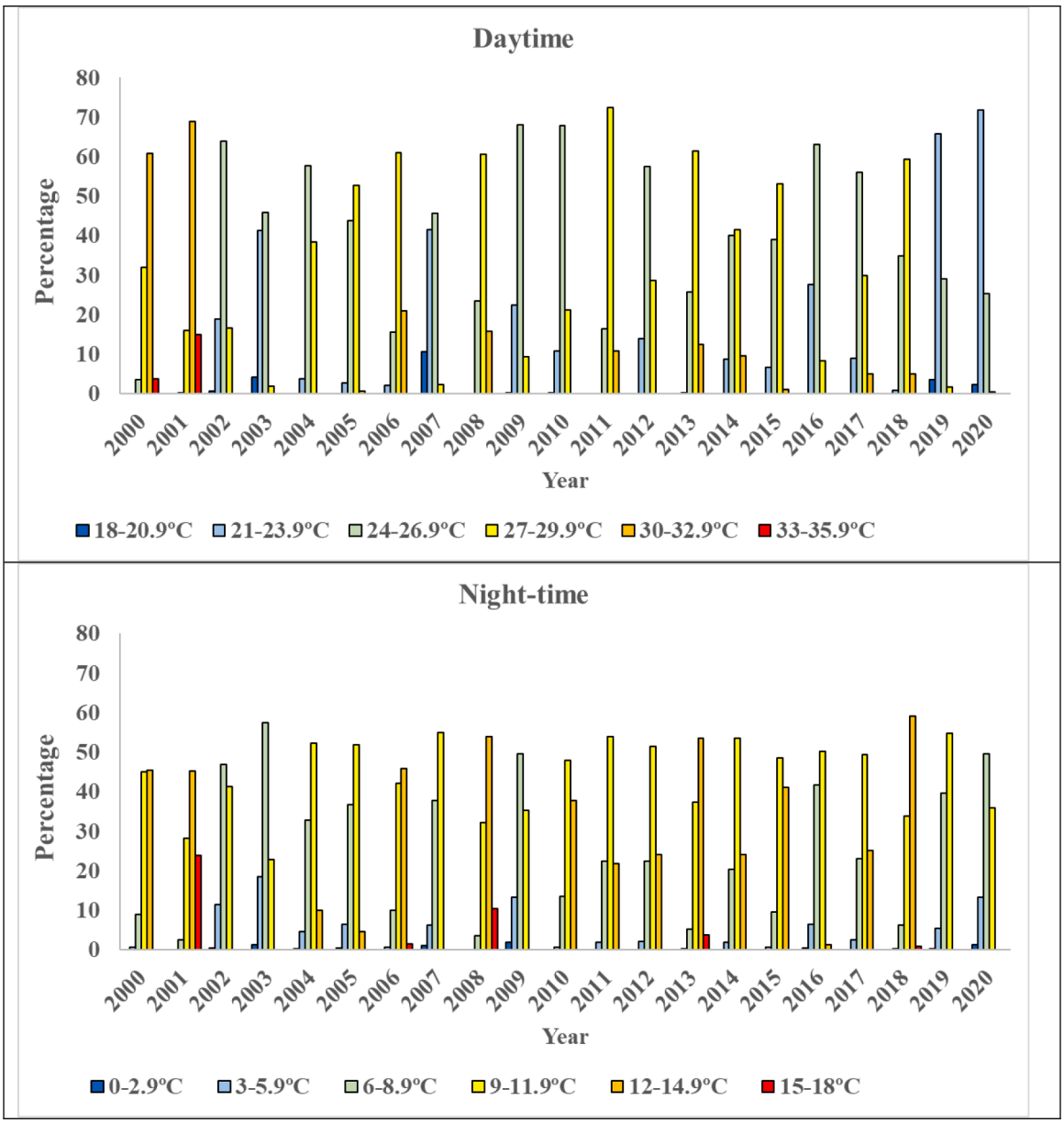

Fig. 8. Percentage area for different daytime and night-time temperature classes in Tehran over the period 20 March to 20 April for each year: 2000–2020.

2001 (83.8%), 2000 (64.6%) and 2006 (21.1%). The year 2020 stands out as the year with the lowest areal extent of urban area (only 0.5%) occupied by heat classes in the range of 27 to 35.9 °C, followed by 2019 (1.7%) and 2003 (2.0%).

For night-time values, on average 5.0% of Tehran experiences mean temperatures in the range of 0 to 5.9 °C during the period 20 March to 20 April over the years 2000–2020 (Fig. 8). Noteworthy is that in the year 2008, which recorded the lowest UHI areal extent, no area fell within this mean night-time 0 to 5.9 °C temperature class, but in fact had the highest mean night-time temperature (15.7 °C) of all years. Conversely, 76% of years record less than 7% areal extent of cold island night-time mean temperatures between 0 and 5.9 °C, yet in the year 2007, which recorded one of the lowest cold island areal extents (20,454 hectares; see Fig. 4), about 7.4% of Tehran fell within this temperature class. In 2020, as much as 14.6% of Tehran's areal extent fell within this mean night-time temperature class, which is the third most extensive area for this class after 2003 (19.7%) and 2009 (15.2%). Largest areal extent of night-time heat islands occurred in 2019 (26,079 hectares) and 2007 (24,911 hectares), yet in both these years no area of the city recorded mean threshold temperatures in the warmest classes of 12 to 18 °C (Fig. 8). These patterns point to the fact that one cannot only consider areal extent of heat or cold islands, as in some years of greater areal coverage of urban heat (cold) islands, a smaller than average portion of the city may have experienced extreme high (low) temperature thresholds. Hence, the importance of considering both areal extent of heat/cold islands and their thermal threshold values.

Findings thus show that maximum variability in the areal extent of the UHI is during daytime (sunshine) hours, coinciding also with maximum economic, social and other activities in Tehran. To this end, results indicate substantial decreases in the areal extent of the UHI during 2020, particularly in areas with 'heavy industry' over western and some portions of southern Tehran. Yet at the same time, the UHI expanded over northern regions of the city where 'open midrise' and 'open low-rise' residential land uses are most prominent. In addition, for the first time we observe the establishment of a cold island over the eastern half of Tehran where 'compact midrise' residences are the dominant land use.

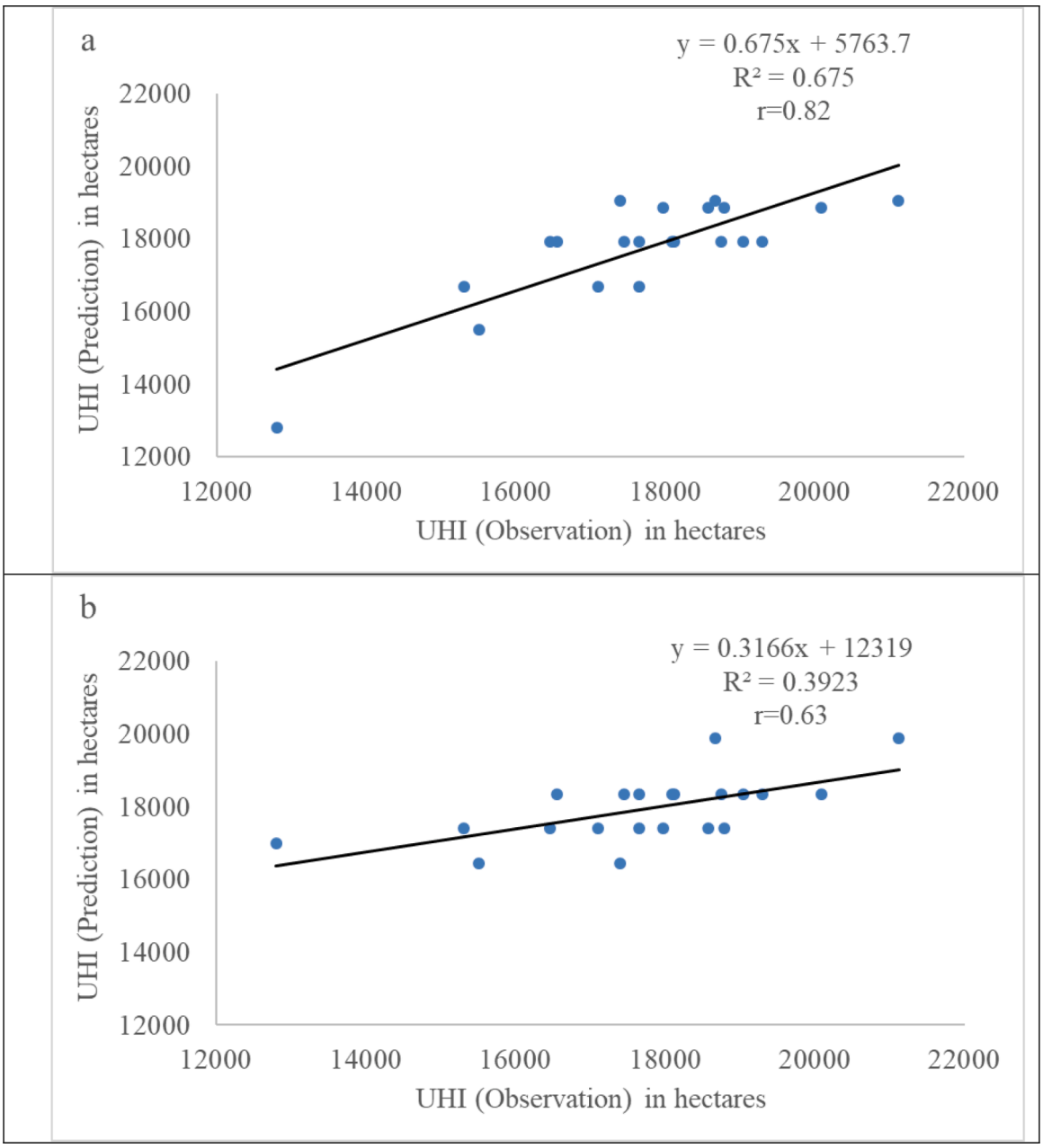

Fig. 9. Changes in the predicted values of the areal extent (hectares) of daytime UHI coverage over Tehran versus the actual values for the period 20 March to 20 April each year (2000 to 2020). a) Predicted areal extent of the UHI according to the 700hPa temperature level and b) Predicted areal extent of the UHI according to the 500hPa temperature level.

4.7. Influence of atmospheric systems on Tehran's UHI

Using the Classification and regression trees (CART) method, we predict changes in the areal extent of the UHI based on temperatures at the 700hPa and 500hPa levels (Fig. 9). Correlation between the *actual* extent of the UHI over Tehran and that for the *predicted* area based on temperatures, indicates significant values of $r = 0.63$ and $r = 0.82$ for the 700hPa and 500hPa levels respectively. Similarly, statistical values for the Nash-Sutcliffe coefficient and RSR were calculated for predicted values at the 700hPa (NSE = 0.67; RSR = 0.57) and 500hPa (NSE = 0.40; RSR = 0.76) levels. These results demonstrate a better performance (less error) at the 700hPa than 500hPa level. The greater distance between the 500hpa level and the ground level means a reduced impact that this temperature level (500hpa) has on the UHI.

Fig. 10 presents patterns of temperature variability for the 500 and 700hPa levels. Long-term average temperatures for the period 20 March to 20 April (1950–2020) at the 500 and 700hPa levels are -18.45 °C and -0.41 °C respectively. In 2020, temperatures at these levels were -18.40 °C and -0.32 °C respectively, thus only fractionally lower than the long-term average. This demonstrates near-normal upper atmospheric conditions during March/April of 2020, and hence no unusual anomaly at these levels or at the synoptic scale. When examining data for the last two to three decades, these indicate temperature equivalents or cooler conditions than those in 2020 for the years 2004, 2007, 2009, 2011, 2012, 2013, 2016 and 2019 at the 500hPa level, and during the years 1992, 1993, 1996, 1997, 1999, 2007, 2012 and 2019 at the 700hPa level. In addition, despite results showing some years with very low temperatures at the 500 and 700hPa levels, this has not yielded smaller areal extents of the UHI than that measured in 2020. For instance, if examined at the 500hPa level, coldest years with average temperatures

Table 8
Percentage probability occurrence of various climatic components using the standard normal distribution method. Probability occurrence values lower than those recorded in 2020 are indicated in red.

Year	UHI	T_{mean}	T_{max}	T_{min}	700hpa	500hpa
2000	90.66	92.65	90.32	91.15	82.12	58.32
2001	55.17	96.41	96.41	94.84	96.08	93.06
2002	57.93	27.76	22.97	37.07	37.07	57.14
2003	80.78	28.1	25.14	39.36	32.28	47.21
2004	58.32	33.72	35.94	30.15	32.28	**32.64**
2005	36.32	32.64	37.45	32.28	59.48	77.64
2006	68.08	76.42	79.95	77.04	81.06	72.91
2007	97.06	17.36	16.85	21.77	**11.7**	**15.63**
2008	72.24	97.67	98.64	98.03	98.57	84.85
2009	42.47	8.08	13.79	**4.09**	**6.81**	**2.44**
2010	48.01	43.64	48.41	47.21	79.1	96.08
2011	30.85	68.08	61.03	66.64	45.62	**35.57**
2012	69.85	52.39	52.79	48.8	**17.62**	**11.12**
2013	43.64	81.86	82.12	78.52	56.36	**31.92**
2014	71.57	37.83	42.86	29.12	42.47	59.1
2015	76.73	57.14	49.2	64.43	55.96	62.93
2016	25.46	22.36	24.2	18.14	41.29	**35.94**
2017	23.89	30.85	25.46	35.57	53.98	70.19
2018	8.89	82.89	80.78	83.15	75.8	86.86
2019	10.75	23.27	18.41	28.43	**2.68**	**2.56**
2020	**0.3**	**4.85**	**4.95**	**4.18**	**28.1**	**35.94**

of -19.81 °C and -19.79 °C were recorded in 2009 and 2019, respectively. These same years had daytime UHI extents of 17,392.75 and 15,511.17 hectares respectively, and all of which were greater in extent than that measured in 2020. Conversely, although the year 2018 was warmer than most at the 500hPa level (av. = -17.02 °C), it produced the smallest UHI extent (15,303 hectares). Similar scenarios occur for temperature patterns at the 700hPa level. Coldest temperatures at the 700hPa level were measured in 1992 (-3.12 °C), 2019 (-1.90 °C), 1996 (-1.63 °C) and 1997 (-1.47 °C), yet in both 1996 and 1997 the UHI extent was greater than that measured in 2020. Interestingly, in 2007, when both the 500hPa (-18.65 °C) and 700hPa (-1.04 °C) levels show cooler temperatures than those in 2020, the daytime UHI was most extensive in area. We demonstrate these examples to show that upper level conditions driven by regional weather patterns (synoptics) are clearly not the only determining factor affecting Tehran's UHI, and that in fact ground-based conditions may in many years have an overriding impact to that of upper atmospheric (synoptic only) conditions.

4.8. Context of climatic conditions in 2020

We now consider the 2020 climate in context of the longer-term mean conditions for the March-April period, based on standard normal distributions. In so doing, we hypothesize a normal distribution and use the Kolmogorov-Smirnov test for verification (see also Alma et al., 2018; Ye, Hanson, Ding, Wang, & Vogel, 2018; Sharma et al., 2019). Probability occurrences of six climate components (i.e. T_{mean}, T_{max} and T_{min} for Mehrabad station; areal extent of the UHI over Tehran; and temperatures at the 700hPa and 500 hPa levels for years 2000–2020) were established (see Table 8) (Fig. 6).

The percentage probability occurrence of the UHI areal extent in 2020 is 0.3% and confirms the lowest probability of occurrence for all years considered here (Table 8). By comparison, other years with low probability values include 2018 (8.89%), 2019 (10.75%) and 2017 (23.89%). The lowest percentage probability occurrences for T_{mean} and T_{max} are also recorded in 2020 (4.85% and 4.95% respectively), and by comparison the second lowest occurrences are measured for the year 2009 (8.08% and 13.79% respectively). However, for T_{min}, the lowest probability of occurrence is calculated for 2009 (4.09%), followed closely by 2020 (4.18%). Our assessment thus demonstrates that the overall lowest probability of such climate component occurrences is for 2020, followed by 2009. Yet, probability estimates for 700hPa temperatures is not particularly low (28.01%) for 2020. By comparison, the years 2009 (2.68%), 2019 (6.81%), 2007 (11.7%) and 2012 (17.62%) record lowest probabilities. Similarly, probability estimates for 500hPa temperatures in 2020 are relatively high (35.94%), with seven years since 2000 recording lower probabilities. This suggests that there was no anomalous regional climatic scenario in 2020, yet near-surface climatology across Tehran was anomalous. The implications of these results are that localized urban-based factors contributed to the anomalous urban climatic scenario in March-April of 2020.

5. Discussion

Although the COVID-19 pandemic has only been with us for 1–2 years, there have already been a number of published articles dealing with (indirect) associated impacts on weather and climate, including likely consequences on current and future global climate (Forster, Forster, & Evans, 2020) and implications for climate crisis management (Manzanedo and Manning, 2020). Studies have also identified regional to sub-regional climate/weather associations with COVID-19, such as over Iran (Ahmadi & Ramezani, 2020) and Jakarta, Indonesia (Tosepu et al., 2020) respectively. Most efforts have focused on climatic parameters that most effectively spread the disease (Adekunle, Tella, Oyesiku, & Oseni, 2020; Doğan, Jebli, Shahzad, Farooq, & Shahzad, 2020; MazharIqbal et al., 2020; Silva, MolinRibeiro, Cocco Mariani, & Santos Coelho, 2020). In contrast, our work has examined how the COVID-19 related lockdown has impacted on urban climate; namely the UHI. To this end, we have demonstrated that the Tehran metropolis experienced relatively immediate climatic responses. Our results demonstrate a few key important findings, which we now summarize.

Perhaps one of the most important spatial contexts of recent climate warming has been in large urbanized areas. Here, heat islands have expanded spatially and become more intense due to the combined effects of both regional climate warming and enhanced urban warming through increased human-induced activities and land-cover change (Huang & Lu, 2015; Roshan & Moghbel, 2020a; Roshan, Moghbel, & Attia, 2020). In the context of Tehran, results indicate that the heat island has expanded over recent decades, most particularly in western and southwestern sectors where this coincides with originally vegetated surfaces having changed to areas now occupied by industrial development and extensive warehouse complexes. For instance, vegetated surfaces between 1986 and 2010 declined by 1.15km^2 over the Tehran metropolis (Sadeghinia, Alijani, & Zeaieanfirouzabadi, 2013). In addition, the portion of built-up areas expanded from 25% in 1988 to 30% in 2010 over the wider metropolis, while 'green spaces' (gardens, parks, forest patches) declined by about 50% between 1988 and 2000 (Bokaeain et al., 2019).

The relatively high inter-annual variation of Tehran's heat island (spatially and intensity) during the March- April period may be due to this being a transitional climatic period (i.e. spring) between the relatively cold months before, and hot months after this time. Hence, the dominance of either cold or warm air masses, both of which typically influence Tehran during this time of year, affecting such inter-annual variability (Azizi, Shamsipour, Mahdian mahforouzi, & Miri, 2014). An additional factor in recent years has been the greater ease with which urban inhabitants of Tehran have been able to travel out of the city during this annual holiday period, which is largely owing to improved road and transport infrastructure. This might account for some of the cooler anomalies and reduced heat island effects in recent years, as opposed to earlier years when fewer people vacated the metropolis.

Our results demonstrate that owing to the month-long 'shut-down' from 20 March to 20 April 2020, there are notable temperature reductions (using a variety of parameters) over those of previous years, as also a reduced areal extent of the UHI across the Tehran Metropolis. We have also demonstrated that cooling during 2020 is not a product of upper atmospheric (i.e. synoptic scale) scenarios, as these indicate relatively normal conditions when compared to the longer-term

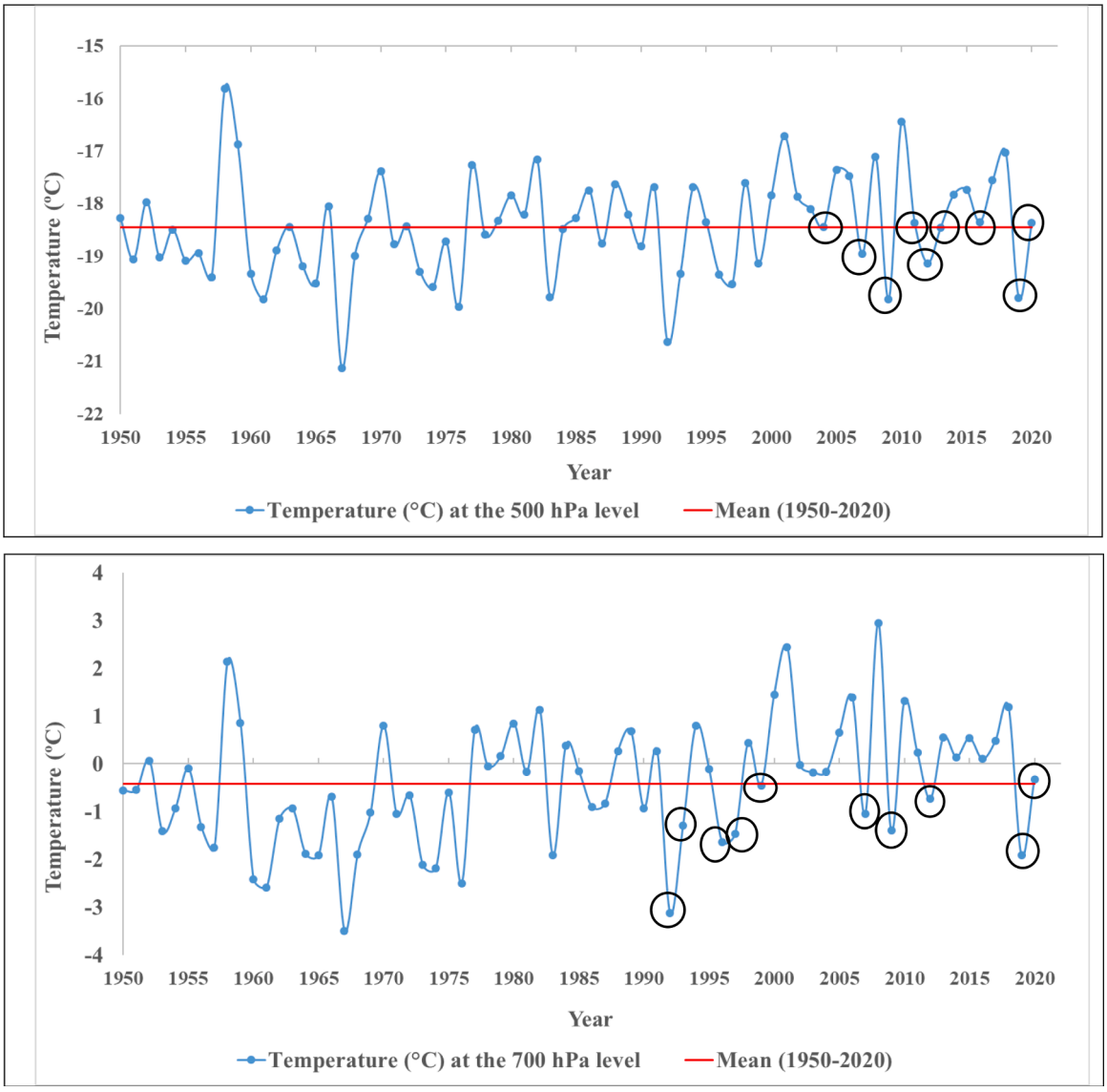

Fig. 10. Temperature variability at the 500 and 700hPa levels over Tehran for the period 20 March to 20 April each year: 1950–2020. Years colder than 2020 are marked with a black circle.

(1950–2020) (Fig. 10). The strongest anomaly is for day-time temperatures (T_{max}), for which there is a recorded temperature departure of -2.72 °C in 2020, while that for T_{min} = -1.15 °C and T_{mean} = -1.87 °C. Strongest temperature reductions during the day may at least in part reflect a more dramatic decline in human-related urban activities during day-time working hours (when there would be maximum production and movement across the city) than during the night when such activities would, even under normal circumstances, have been at a reduced level over those during the day. However, such deviations in temperature are not uniform in amplitude across the greater Tehran metropolis, as this is a function of land-use type (including such things as architectural design of buildings), land-use density and density of people living in urban/sub-urban zones (Jia & Zhao, 2020; Li, Chen, Wang, & Gong, 2019; Roshan & Moghbel, 2020b). To this end, the current study has identified somewhat smaller negative temperature departures from the mean at more outlying areas (e.g. Rodehen and Firozkoh) than in central Tehran during 2020. This is likely owing to increased energy consumption (e.g. heating) in densely populated residential areas, as has also been reported for Barcelona (Spain) in response to COVID-19 lockdown measures (Mozón-Chavarrias et al., 2021). In the case of Tehran, we would expect that the urban-periphery did not cool as substantially given out-migration from more central parts of the city to such periphery areas during the lockdown. Although it is beyond the scope of the current paper to examine these more complex spatio-temporal dynamical causes of urban heat generation and heat release, which affect urban heat budgets, they are nevertheless important considerations worthy of a more detailed future investigation.

Finally, we consider broader urban and peri-urban environmental implications. Human reaction to the COVID-19 pandemic has included forced lockdowns with reduced (relatively short-term) industrial outputs and traffic volumes, fewer/smaller social gatherings, and considerable changes in daily habits (e.g. greater percentage of the workforce working from home). This has yielded largely positive environmental consequences including reduced greenhouse gas emissions, reduced air pollution, cleaner beaches/urban parks and a decline in environmental (urban) noise pollution (Irfan et al., 2021; Somani, Srivastava, Gummadivalli, & Sharma, 2020; Mozón-Chavarrias et al., 2021). It is difficult to project the extent to which society will revert back to past habits or whether a so called 'new normal' will prevail into the foreseeable future as the COVID-19 pandemic eventually wanes in significance. The longer-term societal habits as a legacy to the pandemic will also likely vary geographically. However, it is likely that reduced urban and air

traffic will prevail, at least to some extent, for the near-future. This is largely owing to an increased number of people permanently working from home, and greater emphasis being supported through on-line platforms of communication as opposed to face-to-face meetings.

6. Conclusion

A major challenge to large and rapidly expanding urban centers worldwide, is self-induced urban heating and rising air pollution while global temperatures continue to rise. This is a particular problem faced in regions already experiencing excessive urban heat, and has important implications for continued urban growth in a sustainable manner that considers human health (Gandini et al., 2020). Until now, solutions to curtail rising levels of urban air pollution and UHI has been largely unsuccessful in many developing nation contexts. To this end, forced urban 'lockdowns' due to the COVID-19 pandemic in such city contexts have yielded positive air quality outcomes and reduced the extent/severity of UHI with almost immediate effect. The COVID-19 pandemic, through its impact on reducing human and industrial activity by an imposed countrywide lockdown during the annual March-April holiday period, had a notable overall urban cooling effect over Tehran in 2020. An influential factor reducing the intensity and areal extent of the UHI was reduced traffic load in the Tehran metropolis. This is an important lesson learnt as it implies that UHI can be managed (i.e. reduced in extent and intensity) relatively quickly, and with immediate climatic effects. This offers a potential management tool to reduce periods of severe heat related health risks when urban heat thresholds reach particularly dangerous levels, especially so in a rapidly warming and urbanizing world.

Declaration of Competing Interest

None.

Acknowledgements

The authors work was partially supported by the Golestan University under grant No. 992161. We thank Golestan University for their support in the project. We wish to thank Professors Ghanghermeh and Ranjbar from Golestan University and Prof. Oji from Gilan University for their comments and intellectual guidance, which helped improve an earlier version of the paper.

References

Adekunle, I., Tella, S. A., Oyesiku, K. O., & Oseni, Io. (2020). Spatio-temporal analysis of meteorological factors in abating the spread of COVID-19 in Africa. *Heliyon, 6*(8), e04749.

Aggarwal, P. (2017). 2°C target, India's climate action plan and urban transport sector. *Travel Behaviour and Society, 6*, 110–116.

Ahmadi, K., & Ramezani, M. A. (2020). Iranian emotional experience and expression during the COVID-19 crisis. *Asia-Pacific Journal of Public Health, 32*(5), 285–286.

Ahmed, I., Ahmad, M., & Jeon, G. (2021). Social distance monitoring framework using deep learning architecture to control infection transmission of COVID-19 pandemic. *Sustainable Cities and Society, 69*, Article 102777.

Ali, G., Abbas, S., Qamer, F. M., Wong, M. S., Rasul, G., Irteza, S. M., et al. (2021). Environmental impacts of shifts in energy, emissions, and urban heat island during the COVID-19 lockdown across Pakistan. *Journal of Cleaner Production, 291*, 25806.

Alqasemi, A. S., Hereher, M. E., Kaplan, G., Fadhil Al-Quraishi, A. M., & Saibi, H. (2021). Impact of COVID-19 lockdown upon the air quality and surface urban heat island intensity over the United Arab Emirates. *Science of the Total Environment, 767*, Article 144330.

Ankur, M. M., & Shweta Bhati, P. S. (2020). Urban sprawl during five decadal period over National Capital Region of India: Impact on urban heat island and thermal comfort. *Urban Climate, 33*, Article 100647.

Arikan, B., & Kahya, E. (2019). Homogeneity revisited: Analysis of updated precipitation series in Turkey. *Theoretical and Applied Climatology, 135*, 211–220.

Azizi, G., Shamsipour, A., Mahdian mahforouzi, M., & Miri, M. (2014). Intensities of the Urban Heat Island of Tehran under the influence of atmospheric synoptic patterns. *Journal of Environmental Sciences, 39*(4), 55–66.

Beria, P., & Lunkar, V. (2021). Presence and mobility of the population during the first wave of Covid-19 outbreak and lockdown in Italy. *Sustainable Cities and Society, 65*, Article 102616.

Breiman, L., Friedman, J. H., Olshen, R. A., & Stone, C. J. (1984). *Classification and regression trees*. Monterey: Wadsworth and Brooks/Cole.

Chakraborty, T. C., Sarangi, C., & Lee, X. (2021). Reduction in human activity can enhance the urban heat island: Insights from the COVID-19 lockdown. *Environmental Research Letters, 16*(50), Article 054060.

Chen, Z., Hao, X., Zhang, X., & Chen, F. (2020). Have traffic restrictions improved air quality? A shock from COVID-19. *Journal of Cleaner Production, 279*, Article 123622.

Choubin, B., Zehtabian, G., Azareh, A., Rafiei-Sardooi, E., Sajedi-Hosseini, F., & Kişi, Ö. (2018). Precipitation forecasting using classification and regression trees (CART) model: A comparative study of different approaches. *Environmental Earth Sciences, 77*, 314.

Comarazamy, D. E., Gonzalez, J. E., Luvall, J. C., Rickman, D. L., & Mulero, P. J. (2010). A land-atmospheric interaction study in the coastal tropical city of San Juan, Puerto Rico. *Earth Interactions, 14*, 1–24.

Dadashpoor, H., & Alidadi, M. (2017). Towards decentralization: Spatial changes of employment and population in Tehran Metropolitan Region, Iran. *Applied Geography, 85*, 51–61.

Dai, Z., MichelGuldmann, J., & Hu, Y. (2018). Spatial regression models of park and land-use impacts on the urban heat island in central Beijing. *Science of the Total Environment, 626*, 1136–1147.

Daramola, M. T., & Balogun, I. A. (2019). Local climate zone classification of surface energy flux distribution within an urban area of a hot-humid tropical city. *Urban Climate, 29*, Article 100504.

Doğan, B., Jebli, M., Shahzad, K., Farooq, T., & Shahzad, U. (2020). Investigating the Effects of Meteorological Parameters on COVID-19: Case Study of New Jersey, United States. *Environmental Research, 191*, Article 110148.

Emadodin, I., Taravat, A., & Rajaei, M. (2016). Effects of urban sprawl on local climate: A case study, North Central Iran. *Urban Climate, 17*, 230–247.

ESRI, (2018). How Hot Spot Analysis: Getis-Ord Gi* (Spatial Statistics) works [WWW Document]. URL http://pro.arcgis.com/en/pro-app/tool-reference/spatial-statistics/h-how-hot-spot-analysis-getis-ord-gispatial-stati.htm (accessed 2.21.18).

Forster, P. M., Forster, H. I., & Evans, M. J. (2020). Current and future global climate impacts resulting from COVID-19. *Nature Climate Change, 10*, 913–919.

Georgiana, G., & Uritescu, B. (2018). Spatial hotspot analysis of Bucharest's Urban Heat Island (UHI) using Modis Data, Annals of Valahia University of Targoviste. *Geography Series, 18*(1), 14–22.

Geraldi, M. S., Bavaresco, M. V., Triana, M. A., Melo, A. P., & Lamberts, R. (2021). Addressing the impact of COVID-19 lockdown on energy use in municipal buildings: A case study in Florianópolis, Brazil. *Sustainable Cities and Society., 69*, Article 102823.

Ghanghermeh, A., Roshan, G., Orosa, J. A., Calvo-Rolle, J. L., & Costa, Á. M. (2013). New climatic indicators for improving urban sprawl: A case study of Tehran city. *Entropy, 15*(3), 999–1013.

He, S., Zhang, Y., Gu, Z., & Su, J. (2019). Local climate zone classification with different source data in Xi'an, China. *Indoor and Built Environment, 28*(9), 1190–1199.

Huang, Q., & Lu, Y. (2015). The effect of urban heat island on climate warming in the Yangtze River Delta Urban Agglomeration in China. *International Journal of Environmental Research and Public Health, 12*(8), 8773–8789.

Imai, K., & Yamamoto, K. (2015). An evaluation of measures regarding road traffic against the urban heat island in the Tokyo Ward Area, Japan. *Journal of Environmental Protection, 6*, 957–975.

InácioPortela, C., GiliMassi, K., Rodrigues, T., & Alcântara, E. (2020). Impact of urban and industrial features on land surface temperature: Evidences from satellite thermal indices. *Sustainable Cities and Society., 56*, Article 102100.

Inostroza, M. A. I., & PeileiFan. (2019). Urban sprawl, compact urban development and green cities. How much do we know, how much do we agree? *Ecological Indicators, 96*(2), 3–9.

Irfan, M., Ahmad, M., Fareed, Z., Iqbal, N., Sharif, A., & Wu, H. (2021). On the indirect environmental outcomes of COVID-19: Short-term revival with futuristic long-term implications. *International Journal of Environmental Health Research* ., 1–11.

Isaifan, R. J. (2020). The dramatic impact of Coronavirus outbreak on air quality: Has it saved as much as it has killed so far? *Global Journal of Environmental Science and Management, 6*, 275–288.

Jia, W., & Zhao, S. (2020). Trends and drivers of land surface temperature along the urban-rural gradients in the largest urban agglomeration of China. *Science of the Total Environment, 711*, Article 134579.

Jiang, P., Fu, X., Fan, Y. V., Klemeš, J. J., Chen, P., Ma, S., et al. (2020). Spatial-Temporal Potential Exposure Risk Analytics and Urban Sustainability Impacts related to COVID-19 Mitigation: A Perspective from Car Mobility Behaviour. *Journal of Cleaner Production*, Article 123673.

Kamruzzaman, M., Deilami, K., & Yigitcanlar, T. (2018). Investigating the urban heat island effect of transit oriented development in Brisbane. *Journal of Transport Geography, 66*, 116–124.

Kenawy, A. M., Lopez-Moreno, J. I., McCabe, M. F., Domínguez-Castro, F., Peña-Angulo, D., Gaber, I. M., et al. (2021). The impact of COVID-19 lockdowns on surface urban heat island changes and air-quality improvements across 21 major cities in the Middle East. *Environmental Pollution, 228*, Article 117802.

Kjellstorm, T., & Meng, M. (2016). Impact of climate conditions on occupational health and related economic losses: A new feature of global and urban health in the context of climate change. *Asia-Pacific Journal of Public Health*, 1–10.

Kotharkar, R., & Bagade, A. (2018). Local Climate Zone classification for Indian cities: A case study of Nagpur. *Urban Climate, 24*, 369–392.

László Bart, I. (2010). Urban sprawl and climate change: A statistical exploration of cause and effect, with policy options for the EU. *Land Use Policy, 27*(2), 283–292.
Li, K., Chen, Y., Wang, M., & Gong, A. (2019). Spatial-temporal variations of surface urban heat island intensity induced by different definitions of rural extents in China. *Science of the Total Environment, 669*, 229–247.
Li, Y., Sun, Y., Li, J., & Gao, C. (2020). Socioeconomic drivers of urban heat island effect: Empirical evidence from major Chinese cities. *Sustainable Cities and Society., 63*, Article 102425.
Lima, L., Scalco, V., & Lamberts, R. (2019). Estimating the impact of urban densification on high-rise office building cooling loads in a hot and humid climate. *Energy and Buildings, 182*, 30–40.
Liu, X., Zhou, Y., Yue, W., Li, X., Liu, Y., & Lu, D. (2020). Spatiotemporal patterns of summer urban heat island in Beijing, China using an improved land surface temperature. *Journal of Cleaner Production, 257*, Article 120529.
Mabon, L., Kondo, K., Kanekiyo, H., Hayabuchi, Y., & Yamaguchi, A. (2019). Fukuoka: Adapting to climate change through urban green space and the built environment? *Cities, 93*, 273–285.
Mahato, S., Pal, S., & Ghosh, K. G. (2020). Effect of lockdown amid COVID-19 pandemic on air quality of the megacity Delhi, India. *Science of the Total Environment, 730*, Article 139086.
Manzanedo, R. D., & Manningc, P. (2020). COVID-19: Lessons for the climate change emergency. *Science of the Total Environment, 742*, Article 140563.
MazharIqbal, M., Abidm, I., Hussain, S., Shahzad, N., Waqas, M. S., & JawedIqbal, M. (2020). The effects of regional climatic condition on the spread of COVID-19 at global scale. *Science of the Total Environment, 739*, Article 140101.
Monzón-Chavarrías, M., Guillén-Lambea, S., García-Pérez, S., Montealegre-Gracia, A. L., & Sierra-Pérez, J. (2021). Heating energy consumption and environmental implications due to the change in daily habits in residential buildings derived from COVID-19 crisis: The case of Barcelona, Spain. *Sustainability, 13*, 918.
Nash, J. E., & Sutcliffe, J. V. (1970). River flow forecasting through conceptual models: Part 1-A discussion of principles. *Journal of Hydrology, 10*(3), 282–290.
Nemati, M., Ebrahimi, B., & Nemati, F. (2020). Assessment of Iranian nurses' knowledge and anxiety toward COVID-19 during the current outbreak in Iran. *Archives of Clinical Infectious Diseases, 15*.
Newman, P. (2020). Cool planning: How urban planning can mainstream responses to climate change. *Cities, 103*, Article 102651.
Oke, T. R. (1987). *Boundary layer climates*. London, England: Routledge.
Otmani, A., Benchrif, A., Tahri, M., Bounakhla, M., Chakir, E. M., El Bouch, M., et al. (2020). Impact of Covid-19 lockdown on PM10, SO2 and NO2 concentrations in Salé City (Morocco). *The Science of the Total Environment, 735*, Article 139541.
Rahimzadeh, F., Asgari, A., & Fattahi, E. (2009). Variability of extreme temperature and precipitation in Iran during recent decades. *International Journal of Climatology, 29*, 329–343.
Rodríguez-Urrego, D., & Rodríguez-Urrego, L. (2020). Air quality during the COVID-19: PM2. 5 analysis in the 50 most polluted capital cities in the world. *Environmental Pollution, 266*, Article 115042.
Roshan, G., & Moghbel, M. (2020b). Rain and snow event cooling effect: A comparison on outdoor and indoor thermal comfort in Ardabil, northwest of Iran. *Theoretical and Applied Climatology*. https://doi.org/10.1007/s00704-020-03403-0
Roshan, Gh. R., Shahraki, S. Z., Sauri, D., & Borna, R. (2010). Urban sprawl and climatic changes in Tehran. *Environmental Earth Sciences, 7*(1), 43–52.
Roshan, Gh. (2020). Comparison of impact of climate change on building energy-saving design for two different climates; Metropolitans of Moscow and Tehran. *Journal of the Earth and Space Physics, 45*(4), 89–202.
Roshan, Gh., & Moghbel, M. (2020a). Quantifying the cooling effect of rain events on outdoor thermal comfort in the southern coastal stations of the Caspian Sea. *Journal of Thermal Biology*, Article 102733.
Roshan, Gh., Moghbel, M., & Attia, Sh. (2020). Evaluating the wind cooling potential on outdoor thermal comfort in selected Iranian climate types. *Journal of Thermal Biology, 92*(102660), 1–13.
Sadeghinia, A., Alijani, B., & Zeaieanfirouzabadi, . (2013). Analysis of spatial - Temporal structure of the urban heat island in tehran through remote sensing and geographical information system. *Geography and Environmental Hazards, 1*(4), 1–17.
Sahani, N., Goswami, S. K., & Saha, A. (2020). The impact of COVID-19 induced lockdown on the changes of air quality and land surface temperature in Kolkata city, India. *Spatial Information Research, 29*, 519–534.
Senanayake, I. P., Welivitiya, W. D. D. P., & Nadeeka, P. M. (2013). Remote sensing based analysis of urban heat islands with vegetation cover in Colombo city, SriLanka using Landsat-7 ETM+ data. *Urban Climate, 5*, 19–35.
Sharma, C., & Ojha, CS. P .. (2019). Changes of annual precipitation and probability distributions for different climate types of the World. *Water, 11*(10), 2092.
Silva, J., DaSilva, R. M., & GuimarãesSantos, C. A. (2018). Spatiotemporal impact of land use/land cover changes on urban heat islands: A case study of Paço do Lumiar, Brazil. *Building and Environment, 136*, 279–292.
Silva, R. G., MolinRibeiro, M., Cocco Mariani, V., & Santos Coelho, L. (2020). Forecasting Brazilian and American COVID-19 cases based on artificial intelligence coupled with climatic exogenous variables. *Chaos, Solitons & Fractals, 139*, Article 110027.
Somani, M., Srivastava, A. N., Gummadivalli, S. K., & Sharma, A. (2020). Indirect implications of COVID-19 towards sustainable environment: An investigation in Indian context. *Bioresource Technology Reports, 11*, Article 100491.
Soydan, O. (2020). Effects of landscape composition and patterns on land surface temperature: Urban heat island case study for Nigde, Turkey. *Urban Climate, 34*, Article 100688.
Stewart, L. D., Oke, D. T. R., & Scott Krayenhoff, E. (2014). Evaluation of the 'local climate zone' scheme using temperature observations and model simulations. *International Journal of Climatology, 34*, 1062–1080.
Stewart, L. D., & Oke, T. R. (2012). Local climate zones for urban temperature studies. *Bulletin of the American Meteorological Society, 93*(12), 1879–1900.
Tehran Police Traffic Control Center (TPTCC), (2020). Traffic Reports April 2020, Tehran, Iran.
Teufel, B., Sushama, L., Poitras, V., Dukhan, T., Bélair, S., Miranda-Moreno, L., et al. (2021). Impact of COVID-19-related traffic slowdown on urban heat characteristics. *Atmosphere, 12*, 243.
Timofeev, R. (2004). *Classification and regression trees (CART) theory and applications*. In: Master Thesis. Berlin: Center of Applied Statistics and Economics, Humboldt University.
Tobías, A., Carnerero, C., Reche, C., Massagué, J., Via, M., Minguillón, M. C., et al. (2020). Changes in air quality during the lockdown in Barcelona (Spain) one month into the SARS-CoV-2 epidemic. *The Science of the Total Environment, 726*, Article 138540.
Tosepu, R., Gunawan, J., Effendy, D. S., Ahmad, L. O., Lestari, Hariati, Bahar, H., et al. (2020). Correlation between weather and Covid-19 pandemic in Jakarta, Indonesia. *Science of the Total Environment, 725*, Article 138436.
US Environmental Protection Agency. (2008). Reducing urban heat islands compendium of strategies: urban heat island basics. Washington, DC. *Climate protection partnership division*. US Environmental Protection Agency.
Valipour, M. (2012). Hydro-module determination for Vanaei village in Eslam Abad Gharb, Iran. *ARPN Journal of Agricultural and Biological Science, 7*(12), 968e976.
Valipour, M. (2017). Global experience on irrigation management under different scenarios. *Journal of Water and Land Development, 32*(1), 95e102.
Valipour, M., Banihabib, M. E., & Behbahani, S. M. R. (2013). Comparison of the ARMA, ARIMA, and the autoregressive artificial neural network models in forecasting the monthly inflow of Dez dam reservoir. *Journal of Hydrology, 476*, 433e441.
Wu, L., & Zhang, J. (2018). Assessing population movement impacts on urban heat island of Beijing during the Chinese New Year holiday: Effects of meteorological conditions. *Theoretical and Applied Climatology, 131*(3–4), 1203–1210.
Yamamoto, Y., & Ishikawa, H. (2020). Influence of urban spatial configuration and sea breeze on land surface temperature on summer clear-sky days. *Urban Climate, 31*, Article 100578.
Yao, L., Li, T., Xu, M., & Xu, Y. (2020). How the landscape features of urban green space impact seasonal land surface temperatures at a city-block-scale: An urban heat island study in Beijing, China. *Urban Forestry & Urban Green, 52*, Article 126704.
Ye, L., Hanson, LS.., Ding, P., Wang, D., & Vogel, RM.. (2018). The probability distribution of daily precipitation at the point and catchment scales in the United States. *Hydrology and Earth System Sciences, 22*, 6519–6531.
YuShih, W., Ahmad, S., Chen, Y. C., PingLin, T., & Mabon, L. (2020). Spatial relationship between land development pattern and intra-urban thermal variations in Taipei. *Sustainable Cities and Society, 62*, Article 102415.
Zhang, J., Wu, L., Yuan, F., Dou, J., & Miao, S. (2015). Mass human migration and Beijing's urban heat island during the Chinese New Year holiday. *Science Bulletin, 60*(11), 038–1041.
Zhou, X., Okaze, T., Ren, C., Cai, M., Ishida, Y., Watanabe, H., et al. (2020). Evaluation of urban heat islands using local climate zones and the influence of sea-land breeze. *Sustainable Cities and Society, 55*, Article 102060.
Zhu, R., Wong, M. S., Guilbert, É., & Chan, P. V. (2017). Understanding heat patterns produced by vehicular flows in urban areas. *Scientific Reports, 7*, 16309.